Article

Cell Reports

WNT Activates the AAK1 Kinase to Promote Clathrin-Mediated Endocytosis of LRP6 and Establish a Negative Feedback Loop

Graphical Abstract

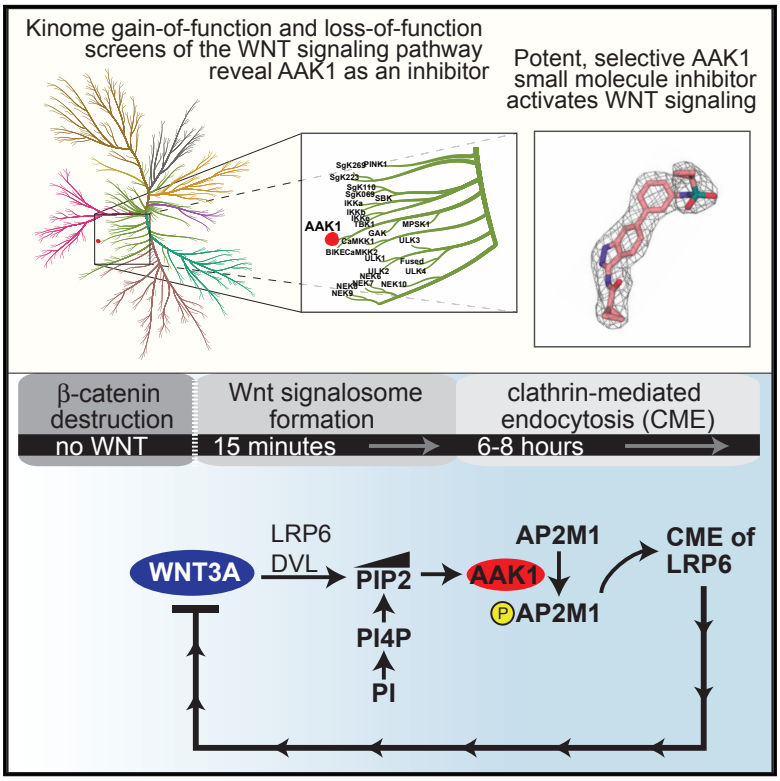

Authors

Megan J. Agajanian, Matthew P. Walker, Alison D. Axtman, ..., Timothy M. Willson, William J. Zuercher, Michael B. Major

Correspondence

benmajor@med.unc.edu

In Brief

WNT signal transduction is essential for normal development and contributes to many human diseases. Agajanian et al. used a kinase gain-of-function screen to show that WNT activates the AAK1 kinase to promote clathrin-mediated endocytosis of the WNT receptor. This work identifies an AAK-driven negative feedback loop that downregulates WNT signaling.

Highlights

- Gain-of-function kinome screen identifies AAK1 as a repressor of WNT signaling
- AAK1 promotes clathrin-mediated endocytosis of LRP6
- Selective AAK1 inhibitor stabilizes β-catenin and activates WNT signaling
- WNT induces AAK1-dependent phosphorylation of AP2M1 and LRP6 endocytosis

Agajanian et al., 2019, Cell Reports *26*, 79–93
January 2, 2019
https://doi.org/10.1016/j.celrep.2018.12.023

CellPress

Cell Reports
Article

WNT Activates the AAK1 Kinase to Promote Clathrin-Mediated Endocytosis of LRP6 and Establish a Negative Feedback Loop

Megan J. Agajanian,[1,2,12] Matthew P. Walker,[1,12] Alison D. Axtman,[3,4,12] Roberta R. Ruela-de-Sousa,[5,12] D. Stephen Serafin,[1,6] Alex D. Rabinowitz,[1] David M. Graham,[6] Meagan B. Ryan,[1,2] Tigist Tamir,[1,2] Yuko Nakamichi,[1,7] Melissa V. Gammons,[8] James M. Bennett,[9] Rafael M. Couñago,[5] David H. Drewry,[3,4] Jonathan M. Elkins,[5,9] Carina Gileadi,[9] Opher Gileadi,[5,9] Paulo H. Godoi,[5] Nirav Kapadia,[3,4] Susanne Müller,[10] André S. Santiago,[5] Fiona J. Sorrell,[9] Carrow I. Wells,[3,4] Oleg Fedorov,[9] Timothy M. Willson,[3,4] William J. Zuercher,[1,3,4] and Michael B. Major[1,2,6,11,13,*]

[1]Lineberger Comprehensive Cancer Center, University of North Carolina at Chapel Hill, Chapel Hill, NC 27599, USA
[2]Department of Pharmacology, University of North Carolina at Chapel Hill, Chapel Hill, NC 27599, USA
[3]Structural Genomics Consortium, UNC Eshelman School of Pharmacy, University of North Carolina at Chapel Hill, Chapel Hill, NC 27599, USA
[4]Division of Chemical Biology and Medicinal Chemistry, UNC Eshelman School of Pharmacy, University of North Carolina at Chapel Hill, Chapel Hill, NC 27599, USA
[5]Structural Genomics Consortium, Universidade Estadual de Campinas – UNICAMP, Campinas, SP 13083-970, Brazil
[6]Department of Cell Biology and Physiology, University of North Carolina at Chapel Hill, Chapel Hill, NC 27599, USA
[7]Institute for Oral Science, Matsumoto Dental University, Nagano 399-0704, Japan
[8]MRC Laboratory of Molecular Biology, Cambridge Biomedical Campus, Cambridge CB2 0SL, UK
[9]Structural Genomics Consortium and Target Discovery Institute, Nuffield Department of Clinical Medicine, University of Oxford, Old Road Campus Research Building, Oxford OX3 7DQ, UK
[10]Structural Genomics Consortium, Buchmann Institute for Molecular Life Sciences, Goethe University Frankfurt, Frankfurt am Main 60438, Germany
[11]Department of Computer Science, University of North Carolina at Chapel Hill, Chapel Hill, NC 27599, USA
[12]These authors contributed equally
[13]Lead Contact
*Correspondence: benmajor@med.unc.edu
https://doi.org/10.1016/j.celrep.2018.12.023

SUMMARY

β-Catenin-dependent WNT signal transduction governs development, tissue homeostasis, and a vast array of human diseases. Signal propagation through a WNT-Frizzled/LRP receptor complex requires proteins necessary for clathrin-mediated endocytosis (CME). Paradoxically, CME also negatively regulates WNT signaling through internalization and degradation of the receptor complex. Here, using a gain-of-function screen of the human kinome, we report that the AP2 associated kinase 1 (AAK1), a known CME enhancer, inhibits WNT signaling. Reciprocally, AAK1 genetic silencing or its pharmacological inhibition using a potent and selective inhibitor activates WNT signaling. Mechanistically, we show that AAK1 promotes clearance of LRP6 from the plasma membrane to suppress the WNT pathway. Time-course experiments support a transcription-uncoupled, WNT-driven negative feedback loop; prolonged WNT treatment drives AAK1-dependent phosphorylation of AP2M1, clathrin-coated pit maturation, and endocytosis of LRP6. We propose that, following WNT receptor activation, increased AAK1 function and CME limits WNT signaling longevity.

INTRODUCTION

β-Catenin-dependent WNT signal transduction is an evolutionarily conserved pathway that instructs cell and tissue-specific differentiation and proliferation programs. It is required for both normal development and maintenance of adult tissue homeostasis (Nusse and Clevers, 2017). Like many developmental signaling pathways, aberrant WNT signaling contributes fundamentally to human diseases, including cancer, bone density disorders, and neurodegeneration (Nusse and Clevers, 2017). The regulation of the WNT/β-catenin signaling axis is often described in three stages: proximal signaling, β-catenin destruction, and nuclear effectors of transcription (Angers and Moon, 2009). In the absence of WNT ligand, the LRP5/6 (low-density lipoprotein receptor related protein 5/6) and Frizzled (FZD) family of WNT receptors remain dissociated. Within the cytosolic compartment, a multi-protein β-catenin destruction complex comprises AXIN1/2, APC (adenomatous polyposis coli), CK1α (casein kinase 1α), and GSK3β (glycogen synthase kinase 3β). CK1α and GSK3β sequentially phosphorylate β-catenin, resulting in its ubiquitylation by β-TRCP and ultimately proteasomal degradation (Hernández et al., 2012; Liu et al., 1999, 2002; Zeng et al., 2005). Extracellular WNT ligand physically couples LRP5/6 and FZD receptors, leading to phosphorylation-dependent recruitment of the DVL (Dishevelled1/2/3), GSK3β, AXIN1/2, and adenomatous polyposis coli proteins (Bilic et al., 2007; Mao et al., 2001; Metcalfe et al., 2010; Tamai et al., 2000). This complex, referred to

as the WNT signalosome, transiently suppresses β-catenin phosphorylation by GSK3β (Bilic et al., 2007). Hence, WNT ligand transiently inactivates the destruction complex to promote cytoplasmic accumulation of β-catenin, resulting in its translocation to the nucleus, where it binds to members of the TCF/LEF family of transcription factors to modulate tissue-specific transcriptional programs and cell phenotypes (Behrens et al., 1996).

Through a gain-of-function screen of the kinome, we discovered that the AP2 associated kinase 1 (AAK1) kinase negatively regulates β-catenin-dependent WNT signaling by promoting clathrin-mediated endocytosis (CME) of LRP6. CME is a complex and multi-step process that removes lipids and transmembrane proteins from the plasma membrane. The assembly polypeptide 2 (adaptor-related protein 2 [AP2]) protein complex first recognizes and binds sorting signals on the intracellular domains of transmembrane cargo proteins (Höning et al., 2005; Ricotta et al., 2002). Activation of the AP2 machine occurs allosterically through binding cargo, clathrin, and PIP2 (phosphatidylinositol 4,5-bisphosphate) (Kadlecova et al., 2017). This activation coincides with a conformational shift in AP2 from "closed" to "open." Open/active AP2 is required for continued clathrin polymerization, cargo recruitment, and ultimately the maturation of a nascent clathrin-coated pit to a stable, successful endocytic event (Conner and Schmid, 2002; Conner et al., 2003; Henderson and Conner, 2007; Kadlecova et al., 2017; Ricotta et al., 2002). In addition to PIP2, cargo, and clathrin, activation of the AP2 complex is promoted by phosphorylation of the AP2M1 subunit by AAK1 (Conner and Schmid, 2002; Conner et al., 2003; Henderson and Conner, 2007; Kadlecova et al., 2017; Ricotta et al., 2002). Importantly, AAK1-dependent phosphorylation of AP2M1 is promoted by clathrin assembly (Conner et al., 2003), which constitutes a positive feedforward loop to promote pit maturation. Once mature, cargo-loaded clathrin-coated pits evolve to endosomal vesicles through dynamin-mediated scission from the plasma membrane (Damke et al., 1994).

Numerous studies establish a regulatory role for CME in WNT signaling, although whether CME activates or inhibits signaling remains debated (Blitzer and Nusse, 2006; Hagemann et al., 2014; Jiang et al., 2012; Kim et al., 2013; Yamamoto et al., 2008). However, a specific role for AAK1 in WNT signaling has not previously been reported. First, clathrin, AP2, and PIP2 are required for WNT-induced LRP6 phosphorylation, signalosome formation, and subsequent WNT signaling (Bilic et al., 2007; Kim et al., 2013). AP2 and clathrin recruitment to the WNT signalosome is induced by WNT ligand, presumably via WNT-induced PIP2 production (Kim et al., 2013). Indeed, WNT ligand induces a gradual accumulation of PIP2 over a 4 hr window after treatment with WNT ligand (Pan et al., 2008). These studies suggest that clathrin-associated machinery is required for WNT-induced signalosome maturation and maintenance and, although not yet proved, possibly for its formation. Second, Gammons et al. (2016a) established that the WNT signalosome incorporates into clathrin-coated pits via DVL polymerization and that this is ultimately required for signalosome formation and WNT signal transduction. Third, De Robertis and colleagues described a mechanism by which the endocytosed signalosome is incorporated into multivesicular bodies (MVBs). Here, sequestration of GSK3β in MVBs suppresses β-catenin phosphorylation, thus potentiating signaling (Taelman et al., 2010). Finally, others have reported that CME of LRP6 and FZD downregulates WNT signaling (Hao et al., 2012; Jiang et al., 2012; Koo et al., 2012; Liu et al., 2014; Yamamoto et al., 2008). For example, disabled homolog 2 (DAB2) drives LRP6 toward CME and represses WNT signaling (Jiang et al., 2012). Additionally, phosphorylation of LRP6 on cytoplasmic tyrosine residues drives CME of LRP6, resulting in decreased WNT signaling (Liu et al., 2014). Furthermore, ubiquitylation of FZD by ZNRF3 and RNF43 drives receptor internalization and degradation, resulting in decreased WNT signaling (Hao et al., 2012; Koo et al., 2012). All together, these studies establish CME as a major regulatory feature in WNT signaling. Although still unresolved, it is likely contextual and temporal considerations play an important role in determining either a positive or negative role for CME in WNT signaling.

Cross-referencing our gain-of-function screen of the kinome with previously published loss-of-function screens, we identify AAK1 as a negative regulator of WNT-induced β-catenin transcription. Gain- and loss-of-function studies reveal that AAK1 negatively regulates WNT signaling by promoting CME of LRP6; FZD remains to be tested. We also report and use a potent and selective cell active AAK1 inhibitor, which potentiates WNT signaling. Full characterization of this small molecule establishes it as the best available tool compound to interrogate AAK1 biology. Unexpectedly, we discovered that WNT induces phosphorylation of AP2M1 by AAK1 in a temporally delayed fashion at 8–10 hr post-WNT3A treatment. Therefore, we propose a modified model whereby WNT-driven CME promotes a negative feedback mechanism to limit pathway longevity. Indeed, we show that WNT stimulation promoted CME of LRP6 in an AAK1-dependent fashion. More broadly, this work contributes to the ongoing discussion of endocytosis within WNT signaling by solidifying a role for the AAK1 kinase in removing LRP6 from the cell plasma membrane.

RESULTS

Identification of AAK1 as a Repressor of WNT Signaling

Thirty years of research on the WNT pathway has revealed its core components and basic mechanics. That said, recent improvements in genetic screening technologies and protein mass spectrometry continue to identify additional modifiers of WNT pathway activity. We, along with others, have reported genome-wide gain- and loss-of-function genetic screens of the WNT pathway, illuminating regulators (e.g., FOXP1, USP6, TFAP4) and their mechanisms of WNT control (Lebensohn et al., 2016; Madan et al., 2016; Walker et al., 2015). Here, we focused on the human kinome to determine which kinases when overexpressed activate or inhibit WNT3A-driven β-catenin transcription. We cloned 387 kinase open reading frames (ORFs) into a lentiviral expression vector before transient overexpression in HEK293T cells carrying the β-catenin-activated Firefly luciferase reporter (BAR) and a constitutively expressed *Renilla* (*Ren*) luciferase. Eighteen hours after kinase transfection, cells were treated with WNT3A conditioned media (CM) for an additional 16 hr before lysis and BAR/*Ren* reporter quantitation (Table S1). ANKRD6/Diversin and CTNNB1/β-catenin served

as positive controls for repression and activation, respectively. Five kinases (AAK1, ADCK1, ADCK2, MAST1, and TGFBR3) were validated by low-throughput reporter assays in HEK293T-BAR/*Ren* cells (Figure 1A). Comparative analysis of this kinome gain-of-function screen in HEK293T cells with two previously published small interfering RNA (siRNA)-based loss-of-function screens in HT1080 sarcoma cells and A375 melanoma cells revealed a single common protein: AAK1 (Table S1) (Biechele et al., 2012; Madan et al., 2016). Because of the well-established functional connections between AAK1 and CME and the emerging data on CME in governing WNT pathway dynamics, we sought to understand how AAK1 negatively regulates the WNT pathway.

To validate and extend the discovery of AAK1 as a WNT inhibitor, we tested (1) whether siRNA-mediated silencing of AAK1 activated β-catenin-driven transcription, (2) the cell-type specificity of the AAK1-WNT phenotype, (3) whether AAK1 regulated the expression of endogenous β-catenin target genes, and (4) whether AAK1 affected the activity of non-WNT signaling pathways. First, in agreement with AAK1 overexpression blocking WNT signaling (Figure 1A), siRNA silencing of AAK1 using two non-overlapping siRNAs increased BAR expression in HT1080 fibrosarcoma cells and RKO colon cancer cells (Figures 1B and 1C). To visualize reporter expression in real time, we silenced AAK1 in HT1080 cells carrying a BAR-mCherry reporter. Quantitation of mCherry fluorescence confirmed that AAK1 knockdown activated the BAR reporter (Figure 1D), while AAK1 overexpression suppressed BAR activity (Figure 1E). Third, to rule out potential reporter-based artifacts, we quantified the expression of two endogenous WNT target genes after AAK1 perturbation. AAK1 knockdown increased RNA expression of *AXIN2* and *NKD1* in both HEK293T and HT1080 cells (Figures 1F and 1G). Conversely, AAK1 overexpression led to decreased RNA expression of *AXIN2* and *NKD1* in HEK293T cells (Figure 1H). Fourth, because of its established roles in CME, AAK1 might broadly regulate other signaling cascades. AAK1 overexpression did not affect TNFα-driven NFκB reporter activity or TGFβ-driven SMAD reporter activity (Figure 1I). Together, these data establish that AAK1 negatively regulates WNT signaling in cells derived from multiple tissue types. Importantly and consistent with its established role in CME, AAK1 did not affect β-catenin transcriptional activity in the absence of exogenous WNT3A stimulation.

Discovery of a Potent and Selective Inhibitor of AAK1

Indazole compound SB-742864 was previously identified as a semi-selective inhibitor of AAK1 (*in vitro* half maximal inhibitory concentration [IC_{50}] = 220 nM) (Elkins et al., 2016). Optimization of SB-742864 via iterative medicinal chemistry optimization led to compound 25A (Figure 2A), a potent and selective inhibitor of AAK1 and the closely related kinase BMP2K. Further optimization to improve the selectivity led to SGC-AAK-1 (Figure 2A), a chemical probe for AAK1 and BMP2K. A closely related molecule, SGC-AAK1-1N (referred to as 34A), which is devoid of activity on AAK1 or BMP2K, was identified for use as a negative control compound. Full details of the chemistry program and analysis of the structure-activity relationships will be published elsewhere. Compounds 25A and SGC-AAK-1, but not 34A, both selectively inhibited AAK1 and BMP2K over the other members of the subfamily, Numb-associated kinases GAK and STK16, in a TR-FRET binding displacement assay (Figures 2B and S1A), with K_i values against AAK1 of 8 and 9 nM respectively for 25A and SGC-AAK1-1 and 2 μM for negative control 34A. Both 25A and SGC-AAK1-1 showed good selectivity over a panel of 406 wild-type protein human protein kinases at 1 μM concentration (Figures 2C and S1B; Table S2) with only a small number of other kinases inhibited with dissociation constant (BMP2K K_D bound to 25A) values within 30 times of those of AAK1. Kinases that exhibited >85% inhibition and/or are common kinase off-targets of acylaminoindazoles within this structural class were analyzed to determine whether the inhibition was confirmed in a dose-dependent K_D determination experiment. Kinases for which the compound of interest demonstrated a K_D < 100 nM are marked with a large red circle and 100 nM < K_D < 1.0 μM with a smaller red circle. One of these kinases, PIP5K1C, is required for PIP2 production, which plays a key role in regulating WNT signaling. To ensure that any observed phenotype is AAK1 dependent, we determined the PIP5K1C IC_{50} values for SGC-AAK1-1 and 34A as 6.6 and 3.6 μM, respectively, in a PIP5K1C enzyme assay at Reaction Biology (Anastassiadis et al., 2011) (Table S3). The *in vitro* IC_{50} values for inhibition of AAK1 enzymatic activity were determined for SGC-AAK1-1 and the negative control (34A) versus a positive control (staurosporine) using a coupled enzyme assay system. Inhibition of AAK1 enzymatic activity was confirmed for SGC-AAK1-1 (IC_{50} = 270 nM). The controls demonstrated the expected activity profiles: 34A was not active (IC_{50} > 1 μM), while staurosporine demonstrated potent AAK1 inhibition (IC_{50} = 120 nM) (Figure S1C). Isothermal titration calorimetry (ITC) measured K_D values for SGC-AAK1-1 of 120 and 490 nM against AAK1 and BMP2K, respectively, and showed that binding had favorable enthalpy (ΔH) and unfavorable entropy (−TΔS) (Figures 2D and S1D; Table S4). Attempts to co-crystallize either inhibitor with AAK1 were unsuccessful, but it was possible to obtain a co-crystal structure of 25A with BMP2K to 2.41 Å resolution (Figures 2E, S1E, and S1F; Table S5). The structure revealed 25A bound in the ATP site, making three hydrogen bonds to the kinase hinge region and two further hydrogen bonds via its sulfonamide oxygens to Gln137 and Asn185, while the central hydrophobic portion of the inhibitor packs against the gatekeeper residue Met130. Hydrogen bonds are indicated as dashed lines to the respective residues within the BMP2K binding pocket (Figure 2E). All pertinent statistics associated with data collection for the BMP2K co-crystal structure, the full-length structure with 25A bound, and the electron density map are included in the Supplemental Information (Table S5; Figures S1E and S1F).

To test that the inhibitors engage AAK1 and BMP2K in live cells, we used NanoBRET assays (Promega) (Vasta et al., 2018), in which human cells were transfected with a plasmid expressing the full-length kinase gene fused to Nanoluc luciferase. In the presence of a fluorescent-labeled ATP-competitive tracer compound, a bioluminescence resonance energy transfer (BRET) signal was measured. Displacement of the tracer by the inhibitor being tested, resulting in loss of BRET, demonstrated target engagement, and linear regression of the IC_{50} values at multiple tracer concentrations yielded the IC_{50} in the absence

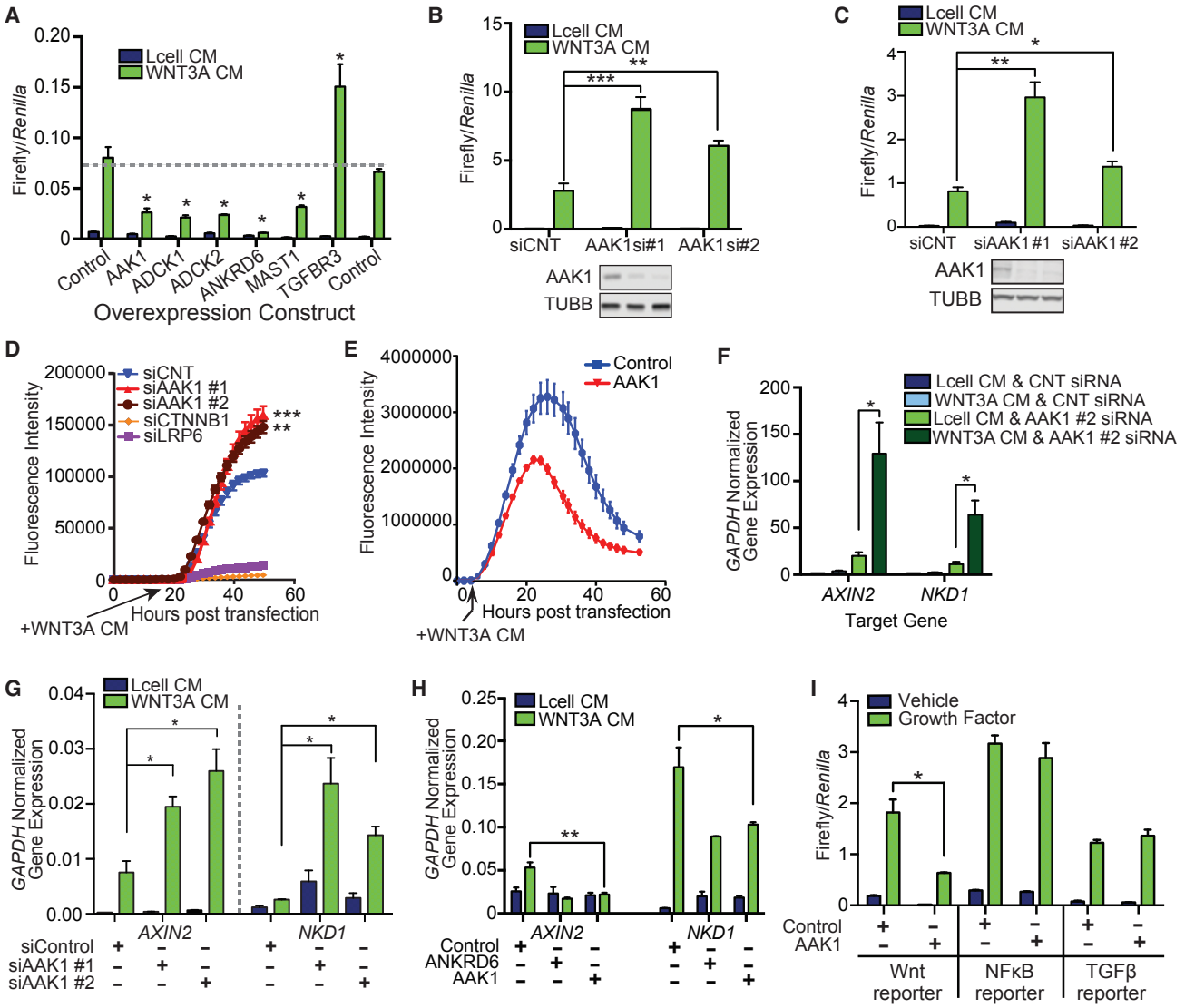

Figure 1. Gain-of-Function Kinome Screen Reveals AAK1 as a Repressor of WNT Signaling

(A) HEK293T-B/R cells were transfected with the indicated construct for 24 hr. Cells were then treated for 16 hr with WNT3A or Lcell CM. Bars represent average Firefly/*Ren* relative fluorescence units (RFU) from three technical replicates.

(B and C) Luciferase assay of HT1080 (B) or RKO (C) stable B/R cells transfected with either control or AAK1 siRNA for 56 hr. Cells were then treated with either Lcell or WNT3A CM for 16 hr. Bars represent average Firefly/*Ren* RFU from three technical replicates. Western blot analysis illustrates knockdown efficiency of two independent AAK1 siRNAs.

(D) IncuCyte imaging of HT1080 cells stably expressing a BAR-mCherry fluorescent reporter transiently transfected with indicated siRNA construct. WNT3A CM was added at 18 hr, then cells were imaged for 50 hr post-transfection. Graph represents data points averaged across four technical replicates.

(E) Live-cell imaging of HT1080 cells stably expressing a BAR-mCherry fluorescent reporter transiently transfected with the indicated expression construct, AAK1, or FLAG control. WNT3A CM was added at 8 hr, and cells were monitored for an additional 56 hr. Data represent the average of four technical replicates.

(F and G) qPCR analysis of *AXIN2* and *NKD1* in HEK293T (F) or HT1080 (G) cells 72 hr after transfection with the indicated siRNA. Cells were treated with WNT3A CM for 6 hr prior to harvest. Bars represent average glyceraldehyde-3-phosphate dehydrogenase (*GAPDH*)-normalized gene expression across three technical replicates.

(H) qPCR analysis of *AXIN2* (left) and *NKD1* (right) in HEK293T cells transfected with overexpression construct for 24 hr, then treated with WNT3A CM for 6 hr prior to harvest. Bars represent average *GAPDH*-normalized gene expression across three technical replicates.

(I) Luciferase assay of HEK293T cells transfected with indicated pathway-specific Firefly luciferase reporter constructs and expression constructs prior to a 16 hr treatment with recombinant human (rh) WNT3A (200ng/mL), rhTNFα (200ng/mL), or rhTGFβ1 (200ng/mL). Bars represent average Firefly/*Ren* RFU from three technical replicates.

*p < 0.05, **p < 0.005, and ***p < 0.0005. All data are representative of biological triplicates, unless otherwise noted. Error bars represent SE.

For complete statistics, see STAR Methods. See also Table S1.

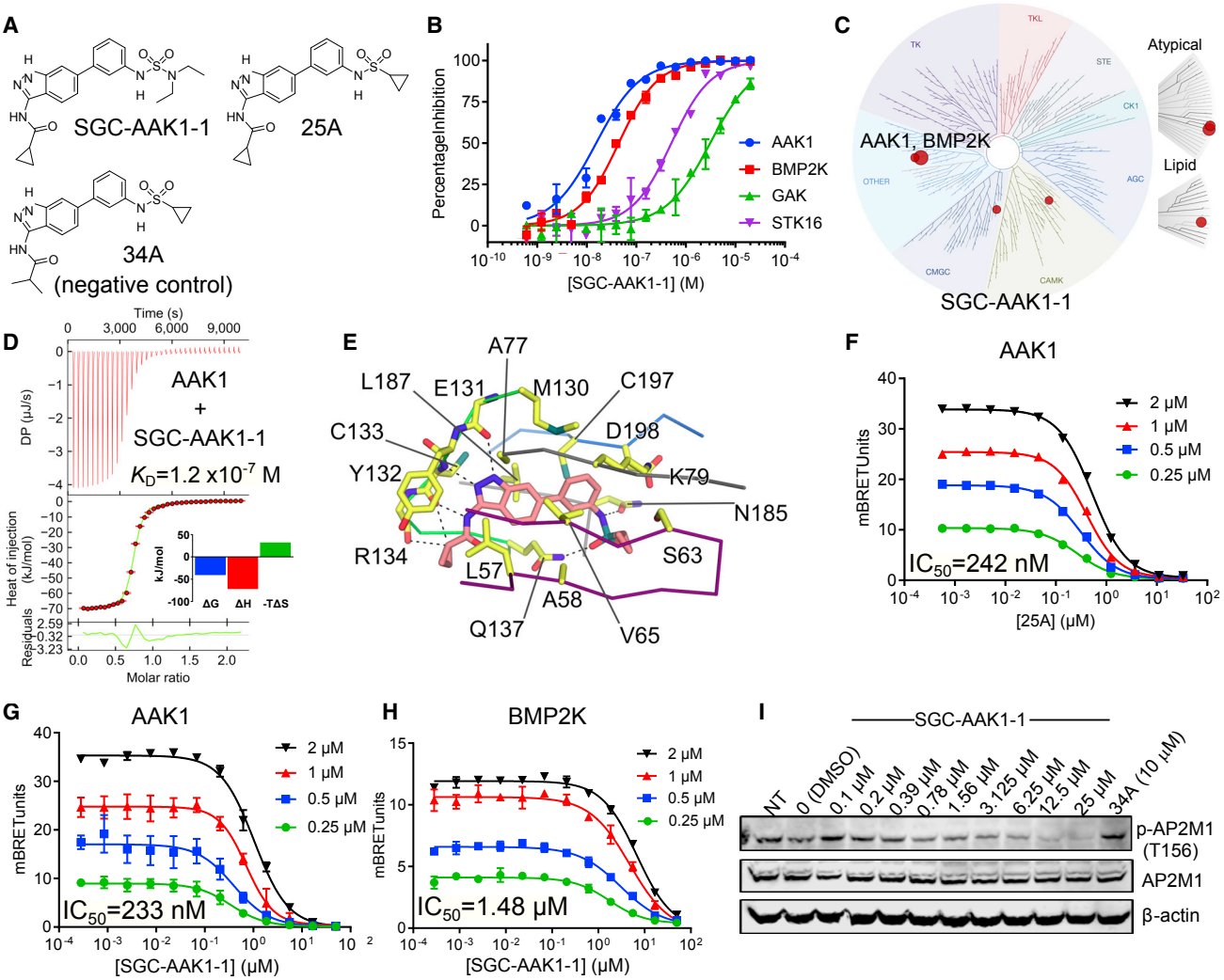

Figure 2. SGC-AAK1-1 Is a Potent and Specific Inhibitor of AAK1 and BMP2K

(A) Chemical structures of the AAK1/BMP2K chemical probe SGC-AAK-1, the related AAK1/BMP2K inhibitor 25A, and the negative control compound 34A that has a similar chemical structure but does not inhibit AAK1 or BMP2K.

(B) SGC-AAK-1 selectively bound AAK1 and BMP2K with a more than 30-fold difference in K_i in a TR-FRET binding displacement assay over the related kinases GAK and STK16. Sixteen-point dose-response curves were measured in duplicate.

(C) SGC-AAK1-1 has good selectivity over the human kinome. SGC-AAK1-1 was used at 1 µM concentration and tested against over 400 wild-type human kinases. K_D determination was completed for all kinases that exhibited >85% inhibition and/or were observed as common off-targets for this structural class. Kinases for which SGC-AAK1-1 has a K_D < 100 nM are marked with a large red circle and 100 nM < K_D < 1.0 µM with a smaller red circle.

(D) ITC confirmed a K_D of 120 nM for binding of SGC-AAK1-1 to AAK1.

(E) A co-crystal structure of BMP2K (2.41 Å) bound to 25A revealed the binding mode of the inhibitor in the ATP site. This structure revealed five key hydrogen bonds and revealed the orientation of the central hydrophobic portion of the inhibitor with respect to the binding pocket.

(F and G) NanoBRET cellular target engagement assays in HEK293T cells showed that 25A (F) and SGC-AAK1-1 (G) both entered cells and directly bound to AAK1 and displaced a fluorescent tracer molecule from the ATP site. Cells were treated with serially diluted inhibitors in the presence of four different concentrations of a NanoBRET tracer molecule, and IC$_{50}$ values were calculated from a linear interpolation of the IC$_{50}$ values at each tracer concentration to obtain the predicted IC$_{50}$ in the absence of tracer. Measurements were made with three technical replicates.

(H) Binding of SGC-AAK1-1 to BMP2K in cells was weaker than to AAK1 with IC$_{50}$ > 1 µM. Displacement of the same fluorescent tracer molecule required increased concentrations of SGC-AAK1-1, revealing an elevated IC$_{50}$ value for binding to BMP2K versus AAK1 in the cellular target engagement assay.

(I) SGC-AAK1-1 inhibited the phosphorylation of the AP2M1 subunit at Thr156 in HEK293T cells in a concentration-dependent manner or with 10 µM 34A. HEK293T cells were treated with inhibitors for 2 hr before western blot analysis.

Error bars represent SE. See also Figure S1 and Tables S2, S3, S4, and S5.

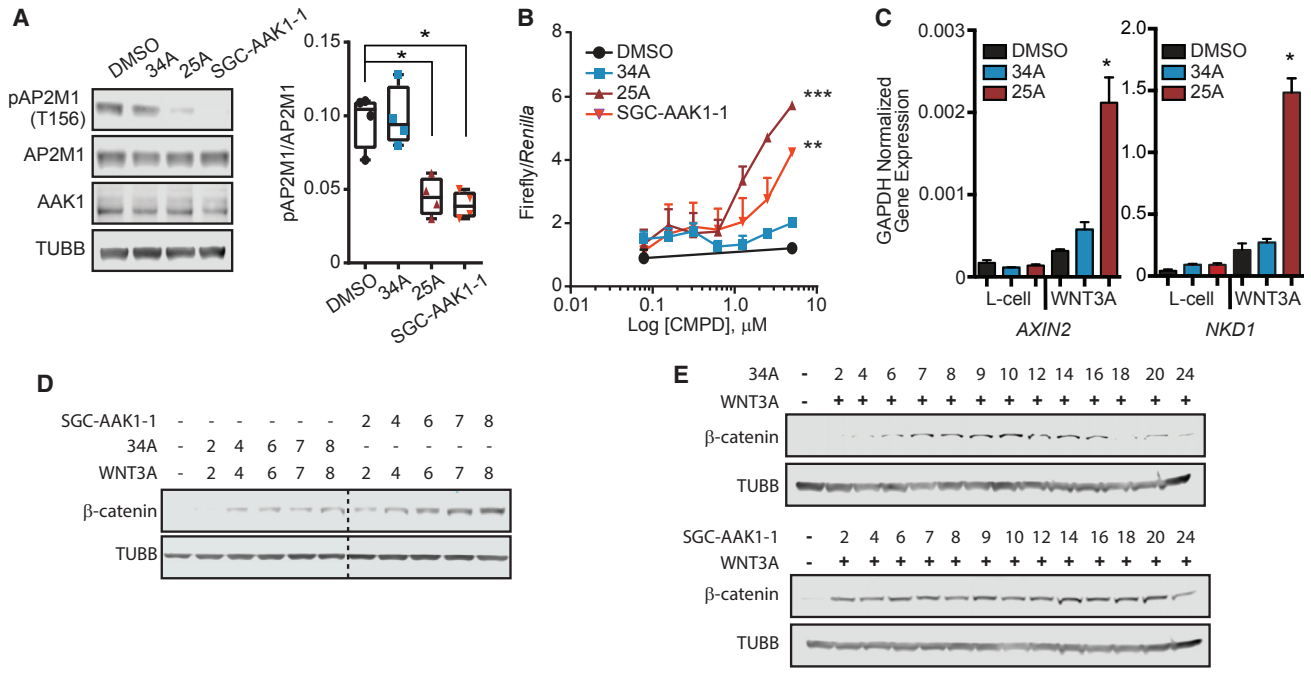

Figure 3. AAK1 Inhibition Potentiates WNT Signaling and Stabilizes β-Catenin

(A) Representative western blot of HT1080 cells treated with indicated compounds (2.5 μM) for 1 hr (left). Box-and-whisker plot represents quantification of four biological replicate experiments using LiCOR software (right).

(B) BAR luciferase assay of HT1080-B/R stable cells treated with WNT3A CM and the indicated dose of compound for 16 hr. Data are averaged over three technical replicates.

(C) qPCR analysis of *AXIN2* or *NKD1* from HT1080 cells treated with indicated compound (1.25 μM) for 12 hr in the presence of Lcell or WNT CM and normalized to *GAPDH*. Graph represents analysis averaged across three technical replicates.

(D and E) Western blot analysis of RKO cells following a 15 min WNT3A pulse, then treated with 1.25 μM of either 34A or SGC-AAK1-1 for the indicated time. Dashed line (D) represents cropped blot for removal of redundant, untreated sample.

*p < 0.05, **p < 0.005, and ***p < 0.0005. All data are representative of biological triplicates, unless otherwise noted. Error bars represent SE. For complete statistics, see STAR Methods.

of tracer. 25A and SGC-AAK-1 bound to AAK1 in HEK293T cells with IC_{50} values of about 240 nM, and more weakly to BMP2K, with IC_{50} values of 600 nM and 1.5 μM, respectively (Figures 2F–2H and S1G). To demonstrate that binding to AAK1 inhibited its enzymatic activity in cells, phospho-AP2M1 (Thr156) levels were observed by western blotting after 2 hr treatment of HEK293T cells with serially diluted SGC-AAK1-1, resulting in a dose-dependent decrease of pAP2M1 starting below 1 μM, in agreement with the NanoBRET data (Figure 2I).

AAK1 Inhibitor Activates WNT Signaling by Stabilizing β-Catenin Levels

To confirm and extend these data, we next tested SGC-AAK1-1 and 25A in a series of experiments to evaluate its potency of AAK1 inhibition in cells and regulation of WNT signaling. First, we treated HT1080 cells with SGC-AAK1-1 and evaluated AAK1-dependent phosphorylation of AP2M1. SGC-AAK1-1, along with 25A, both significantly reduced phosphorylation of AP2M1 (T156), compared with DMSO control and the negative control, 34A (Figure 3A). Second, treatment with SGC-AAK1-1 or 25A activated WNT-driven BAR activity compared with controls (DMSO and 34A) in a dose-dependent manner (Figure 3B). Importantly, 25A also significantly upregulated WNT endogenous target genes *AXIN2* and *NKD1* in HT1080 cells, compared with DMSO control and 34A (Figure 3C). Finally, we measured β-catenin protein abundance following a 15 min pulse of WNT3A ligand in the presence of control compound 34A or SGC-AAK1-1. In cells pulsed with WNT3A and cultured with 34A, β-catenin protein levels increased, reaching a maximum at about 7 hr before returning to baseline at 18 hr (Figures 3D and 3E). In the presence of SGC-AAK1-1, β-catenin protein accumulated more robustly at earlier time points and was sustained throughout the 24 hr time course (Figures 3D and 3E). Together, these results indicate that 25A and SGC-AAK1-1 block AAK1 kinase activity, resulting in increased β-catenin protein stability and β-catenin-dependent transcription.

AAK1 Promotes CME of LRP6 to Inhibit WNT Signaling

Several recent studies report that CME negatively regulates WNT signaling by reducing the presence of the receptor complex on the plasma membrane (Jiang et al., 2012; Liu et al., 2014; Yamamoto et al., 2008). Given the well-established role of AAK1 in phosphorylating AP2M1 to facilitate CME (Conner and Schmid, 2002; Conner et al., 2003; Henderson and Conner, 2007; Ricotta et al., 2002), our discovery of AAK1 as a negative regulator of

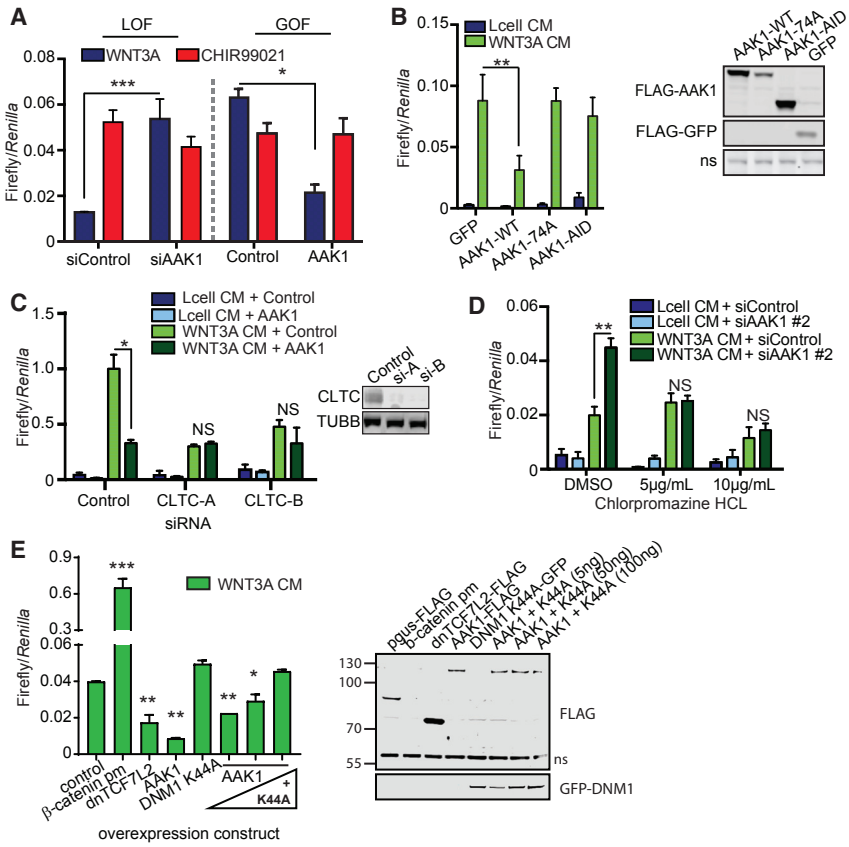

Figure 4. AAK1 Represses β-Catenin-Mediated WNT Signaling through Regulation of Endocytosis

(A) HT1080-B/R cells were transfected with indicated siRNA for 56 hr and then treated with WNT3A or CHIR99021 (1 μM) for 16 hr (left). HT1080-B/R cells were transfected with the indicated overexpression DNA construct and allowed to recover for 12 hr. Cells were then treated with WNT3A CM or CHIR99021 (1 μM) for 16 hr (right). Data are averaged over three technical replicates.

(B) BAR luciferase assay from HT1080 cells transiently transfected with BAR-firefly luciferase, TK-*Ren*, and the indicated expression constructs. Twelve hours post-transfection, cells were treated for 16 hr with Lcell or WNT3A CM and then assayed for BAR activity. Western blot of FLAG-AAK1 and FLAG-GFP is shown to illustrate expression of AAK1 constructs. Presented data are averaged across three technical replicates.

(C) Luciferase assay in HT1080-B/R cells transfected with indicated siRNAs for 50 hr, then co-transfected with indicated expression constructs for 12 hr. Cells were then treated for 16 hr with either Lcell or WNT3A CM. Data are averaged over three technical replicates. Right: western blot of clathrin, indicating knockdown efficiency.

(D) Luciferase assay of HT1080-B/R cells transfected with indicated siRNA for 56 hr, then treated as indicated for 16 hr. Data are averaged over three technical replicates.

(E) Luciferase assay of HEK293T-B/R cells transfected with indicated constructs for 12 hr, then treated with either Lcell or WNT3A CM for 18 hr. β-Catenin pm (point mutant) is a construct with the GSK3β target residues (S33/S37/T41) on β-catenin mutated. Western blot analysis of FLAG and GFP shown to confirm expression of overexpression constructs. Data are averaged over three technical replicates.

*p < 0.05, **p < 0.005, and ***p < 0.0005. All data are representative of biological triplicates, unless otherwise noted. Error bars represent SE. For complete statistics, see STAR Methods.

See also Figure S2.

WNT signaling is not entirely unexpected. That said, AAK1 has not previously been shown to regulate WNT signaling, and certainly, the molecular mechanisms governing CME within the WNT pathway and its homeostasis are not well defined, with several remaining questions and conflicting studies (Blitzer and Nusse, 2006; Gammons et al., 2016a; Hagemann et al., 2014; Jiang et al., 2012; Liu et al., 2014; Taelman et al., 2010; Yamamoto et al., 2008). To confirm that AAK1 functions within membrane proximal steps of WNT signaling, we stabilized β-catenin protein levels with a GSK3β inhibitor (CHIR99021) following either AAK1 overexpression or siRNA silencing. CHIR99021-mediated activation of the BAR reporter was not affected by AAK1 depletion or overexpression (Figure 4A). As expected, β-catenin knockdown blocked BAR activation by AAK1 silencing (Figure S2A). These results indicate that AAK1 functions upstream of β-catenin and the destruction complex. Next, the role of endocytosis in AAK1-mediated repression of WNT signaling was evaluated using two AAK1 mutants: (1) AAK1-74A, which lacks kinase activity, and (2) AAK1-AID, which encodes a truncated form of AAK1 that does not bind the AP2 complex (Conner and Schmid, 2002). Neither AAK1-74A nor AAK1-AID significantly repressed the BAR reporter (Figure 4B), suggesting that both AP2 interaction and kinase activity are required for AAK1-mediated repression of WNT signaling. A role for clathrin and CME in AAK1-driven WNT suppression was tested by (1) siRNA silencing of clathrin, (2) pharmacological inhibition of clathrin-coated vesicles, and (3) blocking dynamin1 function with an established dominant-negative K44A mutation. Two non-overlapping clathrin siRNAs effectively silenced clathrin expression and blocked AAK1-dependent suppression of the BAR reporter in HT1080 cells (Figure 4C). Similarly, treatment with chlorpromazine, an established, albeit promiscuous CME inhibitor (Blitzer and Nusse, 2006; Phonphok and Rosenthal, 1991; Wang et al., 1993) suppressed WNT signaling induced by AAK1 silencing (Figure 4D). Furthermore, co-transfection of AAK1 and dominant-negative dynamin (DNM1) (K44A) rescued the AAK1-induced suppression of BAR activity in a dose-dependent manner (Figure 4E). These experiments suggest that AAK1 represses WNT signaling in a clathrin- and kinase-dependent manner.

We next examined the effect of AAK1 on LRP6 protein levels using cell surface biotinylation assays and flow cytometry. AAK1 overexpression decreased LRP6 protein levels at the plasma membrane (Figure 5A). Additionally, AAK1 knockdown

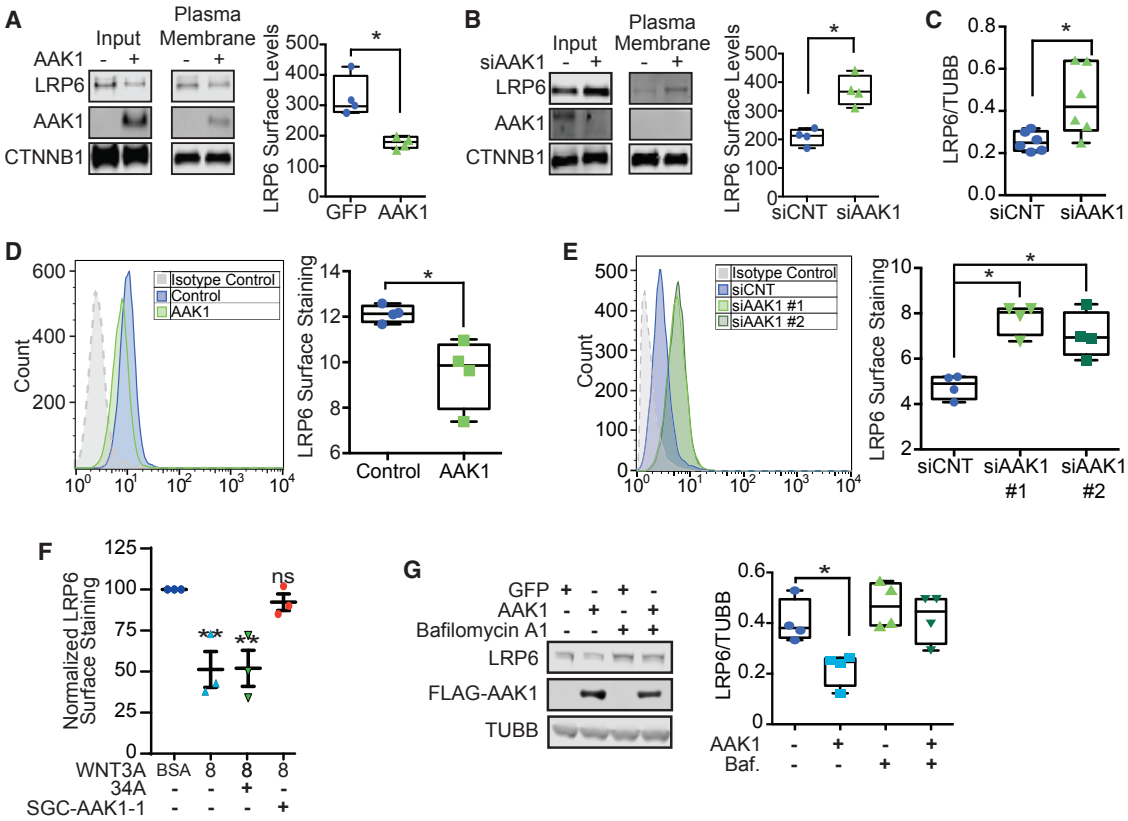

Figure 5. AAK1 Downregulates LRP6 Cell Surface Levels

(A and B) Western blot analysis of HEK293T cells transfected with an AAK1 overexpression construct for 24 hr (A) or AAK1 siRNA for 72 hr (B) prior to membrane fractionation using a surface biotinylation assay. Data represent average surface staining of four biological replicate experiments quantified by LiCOR software.

(C) LiCOR quantification of western blot analysis of LRP6 levels with AAK1 knockdown. The box-and-whisker plot represents total LRP6 expression normalized to β-tubulin (loading control) from six biological replicates quantified by LiCOR software.

(D and E) LRP6 surface staining as detected by flow cytometry analysis in HEK293T cells transfected with an AAK1 overexpression construct for 24 hr (D) or an AAK1 siRNA construct for 72 hr (E). All experiments were quantified using FlowJo software. Experiment was performed in four biological replicates.

(F) LRP6 surface levels as detected by flow cytometry analysis in HEK293T cells treated as indicated for 8 hr. The box-and-whisker plot represents LRP6 surface levels normalized to BSA control for biological triplicates. Raw values for each experiment are shown in Table S6.

(G) HEK293T cells were transfected with FLAG-AAK1 or FLAG-GFP overexpression constructs. Twenty-four hours post-transfection, cells were treated for 6 hr with the autophagy inhibitor bafilomycin A1 (100 nm) or DMSO control prior to cell harvest, then analyzed using western blot for endogenous LRP6 and AAK1 levels. The box-and-whisker plot represents LRP6 expression normalized to β-tubulin from four biological replicates quantified by LiCOR software.

*$p < 0.05$ and **$p < 0.005$. All data are representative of biological triplicates, unless otherwise noted. For complete statistics, see STAR Methods.

See also Figure S3 and Table S6.

by siRNA increased LRP6 surface expression levels (Figure 5B). On the basis of the observation that total LRP6 levels seem to decrease with AAK1 knockdown (Figure 5B), we quantified total LRP6 expression across six biological replicates and demonstrate that with AAK1 knockdown, total LRP6 levels increase (Figure 5C). To validate the changes in surface LRP6 expression findings in an orthogonal assay, we used flow cytometry to quantify cell surface LRP6 levels in HEK293T cells. Here, AAK1 overexpression decreased LRP6 surface levels while AAK1 knockdown increased LRP6 surface levels (Figures 5D and 5E). Importantly, LRP6 surface levels decreased following WNT3A treatment; this decrease was rescued by co-treatment with the active AAK1 inhibitor SGC-AAK1-1, but not the negative control compound 34A (Figure 5F; Table S6). Together, these data indicate that WNT3A treatment decreases LRP6 cell surface levels via an AAK1-dependent mechanism.

We next tested whether AAK1 and LRP6 co-complexed. Using HEK293T cells, immunoprecipitation, and western blot analysis of HA-LRP6 protein complexes revealed the presence of overexpressed FLAG-AAK1 (Figure S3A). Similarly, immunoprecipitation of HA-LRP6 co-purified endogenous AAK1, and reciprocally, immunopurification of overexpressed FLAG-AAK1 revealed co-complexed endogenous LRP6 (Figures S3B and S3C, respectively). Finally, immunoprecipitation of endogenous AAK1 showed co-complexed endogenously expressed LRP6 (Figure S3D). Interestingly, WNT3A stimulation suppressed the association of LRP6 and AAK1 in all experiments (Figures S3A–S3D). Because the AP2 complex is known to associate with LRP6 (Kim et al., 2013), we next tested if AP2M1 was

required for the AAK1-LRP6 interaction. Co-overexpression of AAK1 constructs (WT, 74A, and dAID) and HA-LRP6 followed by FLAG affinity purification and western blot analysis demonstrated that the AAK1 AP2 binding domain is required for the AAK1-LRP6 interaction (Figure S3E).

AAK1 silencing potentiated WNT3A-driven β-catenin activation and increased LRP6 protein levels in whole cell lysate and on the membrane (Figures 5B, 5C, and 5E). Because cargo targeted by CME can be directed to lysosomes for degradation, we tested if the decreased LRP6 levels we observed following AAK1 overexpression were due to CME of LRP6 and subsequent lysosomal degradation. AAK1 was overexpressed in HEK293T cells before treatment with bafilomycin A1, an inhibitor of lysosomal acidification. Western blot analysis established that bafilomycin A1 treatment rescued AAK1-driven downregulation of LRP6 (Figure 5G). Together, these results suggest that AAK1 inhibits WNT signaling by inducing CME endocytosis and lysosomal degradation of LRP6.

WNT3A Induces AAK1 Phosphorylation of AP2M1

Within 15–30 min of WNT3A treatment, LRP6 is phosphorylated by GSK3β and CK1γ (casein kinase 1γ), resulting in transient suppression of β-catenin phosphorylation and degradation (Hernández et al., 2012; Liu et al., 1999, 2002; Zeng et al., 2005). Extended duration of WNT3A stimulation of 4–6 hr results in MVB formation and sequestration of GSK3β (Taelman et al., 2010). Here we asked if WNT3A treatment regulated AAK1-dependent phosphorylation of AP2M1. Time-course analysis in HT1080 or HEK293T cells revealed WNT3A-induced phosphorylation of AP2M1 at 8–10 hr post-treatment, with no change in total AP2M1 or AAK1 protein levels (Figure 6A). To rule out artifacts due to the use of WNT3A CM and to extend relevance to a second cell type, we treated HT1080 cells (Figure S4A) and HEK293T (Figure S4B) cells with recombinant human WNT3A (rhWNT3A) over a time course of 4–16 hr. Western blot analysis revealed an increase in pAP2M1 protein levels 8–10 hr post-WNT3A stimulation. We also tested the importance of continued exposure to WNT ligand over the time course compared with transient pulse of WNT3A. Here, cells were treated with WNT3A for 15 min before replacement with fresh media (Figures S4C and S4D). These experiments demonstrated that a pulse of WNT3A induced a similar increase in AP2M1 phosphorylation compared with continuous exposure to WNT3A ligand.

The WNT3A-induced phosphorylation of AP2M1 required AAK1 expression and activity. First, HT1080 cells or HEK293T cells were treated with WNT3A CM and the AAK1 inhibitor 25A before western blot analysis of phosphorylated AP2M1; 25A blocked WNT3A-induced phosphorylation of AP2M1 (Figures S4C and S4D). Additionally, the AAK1 inhibitor blocked WNT3A-induced AP2M1 phosphorylation when added at any time point following WNT3A treatment (Figure S4E). Second, siRNA silencing of AAK1 also suppressed WNT3A-induced phosphorylation of AP2M1 (Figure 6B). These data suggest that at 8–10 hr post-WNT3A treatment, AAK1-dependent phosphorylation of AP2M1 increases to form a negative feedback loop of CME of LRP6 to decrease its abundance on the plasma membrane.

Intrigued with the delayed WNT3A-induced phosphorylation of AP2M1 by AAK1, we performed a series of functional assays to identify requisite signaling events. First, we found that AAK1-mediated pAP2M1 accumulation was induced by rhWNT3A (3A) and rhWNT5A (5A), the latter of which signals in a β-catenin-independent fashion (Figure 6C). Second, inhibition of GSK3β with CHIR99021 did not result in elevated pAP2M1 levels, suggesting that WNT3A-induced pAP2M1 did not require β-catenin-dependent transcription (Figure 6D). In agreement with these data, inhibiting β-catenin-dependent transcription with overexpressed dominant-negative TCF7L2/TCF4 (dnTCF7L2/dnTCF4) did not affect pAP2M1 increase (Figure 6E). Third, using HEK293T cells lacking all three DVL proteins via CRISPR-Cas9 triple-knockout (TKO) cells (clones 4 and 6) (Gammons et al., 2016b) and HEK293T LRP5/6 CRISPR-Cas9 double-knockout (DKO) cells, we tested whether WNT3A promoted phosphorylation of AP2M1 (Figure 6F). In the absence of LRP5/6 or DVL, AP2M1 phosphorylation did not increase following WNT treatment. Interestingly, background pAP2M1 levels are increased in both LRP5/6 DKO and DVL TKO cells compared with WT HEK293T cells (Figure 6F). Fourth, previous studies established that PIP2 levels increase following short-term (4 hr) WNT3A treatment and that PIP2 is required for WNT signalosome formation (Kim et al., 2013; Pan et al., 2008). Furthermore, PIP2 recruits AP2 to the signalosome, leading to CME of LRP6 (Kim et al., 2013). Thus, we hypothesized that PIP2 is required for WNT3A-induced phosphorylation of AP2M1 by AAK1. To test this hypothesis, we inhibited PIP2 by treating cells with neomycin or carbachol, both of which block PIP2 signaling (Baron et al., 1993; Huang et al., 1999). Treatment of HT1080 cells with neomycin or carbachol blocked WNT3A-induced phosphorylation of AP2M1 (Figure 6G). Furthermore, we blocked PIP2 production by silencing the PI4K2α kinase with two non-overlapping siRNAs. PI4K2α phosphorylates phosphatidylinositol (PI) to phosphatidylinositol 4-phosphate (PI4P) and is required for subsequent PIP2 production (Toker, 1998). In agreement with the neomycin or carbachol experiments, PI4K2α silencing in HT1080 cells blocked WNT3A-dependent increase in pAP2M1 (Figure 6H). We conclude that WNT ligands drive AAK1-dependent phosphorylation of AP2M1 in a manner that is (1) temporally delayed from signalosome formation, (2) independent of β-catenin-mediated transcription, (3) dependent on LRP5/6 and DVL protein expression, and (4) dependent on PIP2 production.

DISCUSSION

CME is a well-established regulator of WNT signaling, although whether CME promotes or inhibits the WNT pathway remains debated (Bilic et al., 2007; Blitzer and Nusse, 2006; Gammons et al., 2016a; Kim et al., 2013; Pan et al., 2008; Taelman et al., 2010; Yamamoto et al., 2008). Certainly, contextual and temporal features in CME-directed WNT studies are important. As a central and positive regulator of CME, our discovery of AAK1 as a WNT modulator is no surprise. Collectively our data show that AAK1 negatively regulates β-catenin-dependent WNT signaling through CME endocytosis of LRP6. Although the experiments have not yet been done, we speculate that FZD is similarly targeted by AAK1 and CME. In the course of our studies,

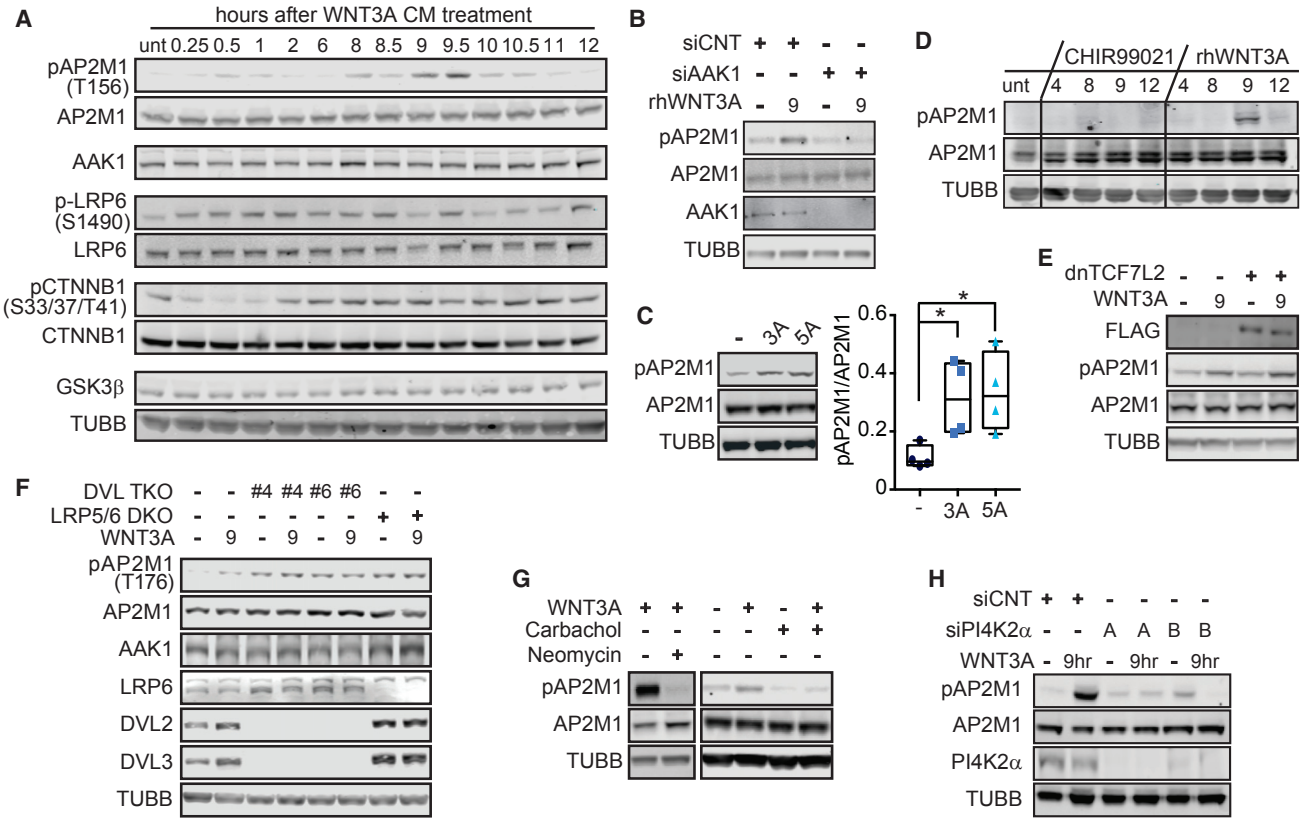

Figure 6. WNT Treatment Induces AAK1-, PIP2-Dependent Phosphorylation of AP2M1

(A) Western blot analysis of HT1080 cells treated with WNT3A CM for indicated times.

(B) Western blot analysis of HT1080 cells transfected with either AAK1 or control siRNA for 72 hr. Cells were then treated with rhWNT3A (200 ng/mL) for 15 min, then the medium was changed for fresh, complete DMEM, and cells were incubated for 9 hr.

(C) Western blot analysis of pAP2M1 levels in HEK293T cells treated with either rhWNT3A (3A) or rhWNT5A (5A) (200 ng/mL) for 9 hr. The box-and-whisker plot represents pAP2M1/AP2M1 expression from four biological replicates quantified by LiCOR software.

(D) Western blot analysis of HT1080 cells treated with either CHIR99021 compound (1 μM) or rhWNT3A (200 ng/mL) for the indicated time.

(E) HEK293T cells were transfected with FLAG-dnTCF7L2 for 24 hr. Cells were then treated with WNT3A for 15 min, then the medium was changed for fresh, complete DMEM, incubated for 9 hr, and analyzed using western blot.

(F) Western blot analysis of HEK293T WT, DVL TKO clone #4, DVL TKO clone #6, and LRP5/6 DKO cells treated with WNT3A CM for 9 hr.

(G) Western blot analysis of HT1080 cells treated with WNT3A CM for 15 mins, then the medium was changed for complete DMEM containing either carbachol (50 μM) or neomycin (100 μM). Cells were incubated for 9 hr prior to cell harvest.

(H) Western blot analysis of HT1080 cells transfected with siRNA against PI4K2α for 72 hr and pulsed with WNT3A CM for 15 mins and then incubated for 9 hr.

All panels are representative of biological triplicates, unless otherwise noted. For complete statistics, see STAR Methods.

See also Figure S4.

we discovered an unexpected WNT-induced phosphorylation event on T156 of AP2M1. This was mediated by AAK1 and reproducibly occurred at 8–10 hr post-WNT treatment. In Figure 7, we summarize our findings in a multi-step model that integrates WNT-driven signalosome formation, PIP2 production, AAK1, AP2M1 phosphorylation, and CME of LRP6.

In the absence of WNT ligand, FZD and LRP6 remain dissociated, allowing β-catenin phosphorylation, ubiquitylation, and degradation (Liu et al., 1999; Liu et al., 2002). Within minutes of WNT stimulation, the WNT signalosome forms, resulting in transient repression of β-catenin phosphorylation by GSK3β (Figure 7A) (Bilic et al., 2007). A key step in signalosome formation is recruitment of the signalosome to nascent clathrin-coated pits with high local concentrations of DVL, which allows the dimerization of DVL, thus potentiating WNT signaling (Gammons et al., 2016a). The newly formed WNT signalosome requires PIP2 for assembly and contains both clathrin and AP2 (Figure 7A) (Pan et al., 2008). On the basis of our data, we suggest that long-term (8–10 hr) WNT stimulation induces a spike in AAK1-dependent phosphorylation of T156-AP2M1. This promotes clathrin polymerization, clathrin-coated pit stabilization and ultimately CME of LRP6, thus constituting a WNT-driven and AAK1-dependent negative feedback loop.

Central to our model is the increase in phosphorylated AP2M1 levels at 8–10 hr post-WNT treatment. Phosphoinositide is converted to PIP2 by PI4K2α and PIP5K (Toker, 1998). Importantly, PIP5K1 association with the DIX domain of DVL1/2/3 results in activation of PIP5K1 (Hu et al., 2015; Pan et al., 2008). One

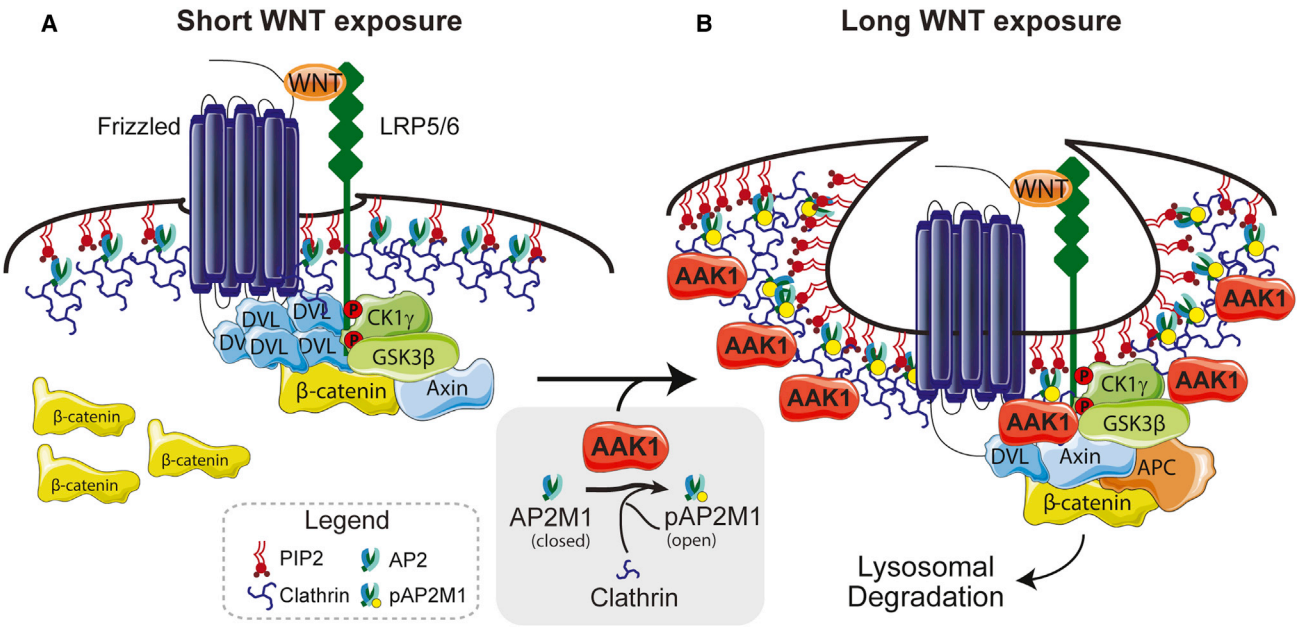

Figure 7. Proposed Model for AAK1-Dependent and CME of LRP6

(A) Within minutes of WNT ligand exposure, FZD and LRP5/6 co-complex, allowing formation of the LRP6 signalosome in nascent clathrin-coated pits. Signalosome formation requires DVL domain swapping and polymerization, as well as PIP2 and AP2 recruitment. This promotes accumulation of β-catenin and activation of the WNT signaling pathway.

(B) Prolonged exposure to WNT ligand drives AAK1-dependent AP2M1 phosphorylation, CME, and ultimately removal of the WNT receptors from the plasma membrane.

hypothesis is that through this mechanism, WNT-driven recruitment of DVL to the LRP/FZD receptor complex results in a time-dependent increase in local PIP2 production. PIP2 and cargo proteins allosterically activate the AP2 complex, thus driving clathrin polymerization and maturation of clathrin-coated pits (Höning et al., 2005; Kadlecova et al., 2017). Phosphorylation of AP2M1 by AAK1 stabilizes the AP2 complex in an open/active confirmation, promoting the binding of clathrin and cargo proteins and ultimately enhancing CME (Figure 7B) (Conner et al., 2003). Although we do not yet understand the mechanistic details, we speculate that PIP2 levels continue to rise hours after WNT stimulation, possibly triggering an increase in AAK1-dependent phosphorylation of AP2M1 and CME of LRP6 (Figure 7B). Further studies that quantify PIP2 levels at 8–10 hr post-WNT stimulation are needed.

Alternatively, the AP2 complex has been reported to cycle between phosphorylated and dephosphorylated states during CME and that this cycling is necessary for robust CME (Kadlecova et al., 2017). Therefore, it is possible that WNT stimulation shifts the AAK1/phosphatase balance to favor phosphorylated AP2M1. Another possibility is AAK1 itself is phosphorylated, either via AAK1 autophosphorylation or phosphorylation by another kinase, resulting in increased AAK1 activity, AP2M1 phosphorylation, and CME of LRP6. Interestingly, previous studies demonstrated that GSK3β inhibition results in increased dynamin-1 activity, leading to rapid and dysregulated CME (Liberali et al., 2014; Reis et al., 2015). It is possible that GSK3β sequestration within MVBs (Taelman et al., 2010) and increased AAK1 activity both contribute to WNT-driven CME of LRP6. Last, given the delayed nature of the AAK1-AP2M1 phospho-event, we were surprised that β-catenin-dependent transcription was not required. Indeed, we also show that the β-catenin-independent WNT ligand WNT5A similarly induces pT156-AP2M1. Interestingly, previous studies demonstrated that an interaction between DVL2 and AP2 is required for WNT5A-induced FZD4 endocytosis (Yu et al., 2007). Together, these data suggest a regulatory role for AAK1 in FZD endocytosis. Although not yet validated *in vivo*, we hypothesize that in certain developmental or disease contexts, WNT-induced pT156-AP2M1 may establish a negative feedback loop to remove LRP/FZD from the cell membrane. Collectively, the molecular events suggested in this time-delayed model are consistent with the timing reported in the GSK3-sequestration model proposed by De Robertis and colleagues (Taelman et al., 2010).

The AP2 complex binds Yxxϕ or dileucine motifs within the intracellular domains of transmembrane cargo proteins (Chen et al., 1990; Collawn et al., 1990). Through phosphorylation of T156-AP2M1, AAK1 was previously shown to promote association of the AP2 complex with cargo (Ricotta et al., 2002). Interestingly, in co-immunoprecipitation experiments, we discovered AP2 regulates the association between AAK1 and LRP6. AP2 interacts with LRP6 through a conserved Yxxϕ motif, which is required for WNT signalosome formation (Gammons et al., 2016a; Kim et al., 2013). We also report that the AAK1-LRP6 co-complex dissipates following WNT3A treatment. Although further experimentation is needed to define the dynamics of

protein-protein interactions during signalosome formation and CME, it is possible that following AAK1-dependent phosphorylation of AP2M1, AAK1 dissociates from the LRP6/AP2 complex.

AAK1 contributes to several neurological disorders, including neuropathic pain, Alzheimer's disease, Parkinson's disease, schizophrenia, and amyotrophic lateral sclerosis (Kostich et al., 2016; Shi et al., 2014). AAK1 has a described role in dendrite branching and spine development (Ultanir et al., 2012), and through the regulation of Neuregulin1/ErbB4, AAK1 has been linked to schizophrenia (Kuai et al., 2011). Just recently, the LX9211 AAK1 inhibitor passed phase 1 clinical trials for neuropathic pain. Here we report the development of a potent and selective AAK1 pharmacological inhibitor (SGC-AAK1-1). SGC-AAK1-1 demonstrates improved biochemical selectivity over the phase 1 clinical agent LX9211 and is confirmed to be cell active. Thus, we report the best available chemical tool to study AAK1/BMP2K pathways and related biology. Like the lead compound 25A, SGC-AAK1-1 inhibited AAK1-dependent phosphorylation of AP2M1 and activated WNT signaling. Looking forward, *in vitro* and *in vivo* neural-directed studies of SGC-AAK1-1 and its comparison with LX9211 are needed to evaluate the therapeutic potential of SGC-AAK1-1. Furthermore, while we describe a role for AAK1 in negatively regulating WNT signaling, AAK1 also inhibits Neuregulin1/ErbB4 and positively regulates the NOTCH pathway (Gupta-Rossi et al., 2011; Kuai et al., 2011). Therefore, AAK1 inhibitors may also regulate these signaling cascades and consequently prove therapeutically beneficial in diseases with misregulated NOTCH or Neuregulin1/ErbB4 signaling. In cancer, mutation and altered expression of several genes promote WNT receptor stability on the plasma membrane, resulting in hyperactive WNT signaling and tumorigenesis (e.g., ZNRF3/RNF43 and USP6; Hao et al., 2012; Koo et al., 2012; Madan et al., 2016; Ruffner et al., 2012; Schmid, 2017). Whether AAK1 expression or activity is suppressed in cancer and if this contributes to WNT activation remain to be determined.

STAR★METHODS

Detailed methods are provided in the online version of this paper and include the following:

SUPPLEMENTAL INFORMATION

Supplemental Information includes four figures and seven tables and can be found with this article online at https://doi.org/10.1016/j.celrep.2018.12.023.

ACKNOWLEDGMENTS

M.B.M. acknowledges support from the NIH (RO1-CA187799 and U24-DK116204-01). M.J.A. received financial support from NIH T32 Predoctoral Training Grants in Pharmacology (T32-GM007040-43 and T32-GM007040-42), an Initiative for Maximizing Student Diversity Grant (R25-GM055336-16), and the NIH National Cancer Institute (NCI) NRSA Predoctoral Fellowship to Promote Diversity in Health-Related Research (F31CA228289). M.P.W. received support from the Lymphoma Research Foundation (337444) and the NIH (T32-CA009156-35). Y.N. was supported by grants-in-aid from the Japan Society for the Promotion of Science (JSPS) (15KK0356 and 16K11493). T.T. was supported by the Howard Hughes Medical Institute Gilliam Fellowship for Advanced Study. M.V.G. was supported by Cancer Research UK (grants C7379/A15291 and C7379/A24639 to Mariann Bienz). The UNC Flow Cytometry Core Facility is supported in part by Cancer Center Core Support Grant P30 CA016086 to the UNC Lineberger Comprehensive Cancer Center, and research reported in this publication was supported by the Center for AIDS Research (award number 5P30AI050410), and the content is solely the responsibility of the authors and does not necessarily represent the official views of the NIH. The Structural Genomics Consortium (SGC) is a registered charity (number 1097737) that receives funds from AbbVie, Bayer Pharma AG, Boehringer Ingelheim, the Canada Foundation for Innovation, the Eshelman Institute for Innovation, Genome Canada, the Innovative Medicines Initiative (European Union [EU]/European Federation of Pharmaceutical Industries and Associations [EFPIA]) (ULTRA-DD grant no. 115766), Janssen, Merck & Company, Merck KGaA, Novartis Pharma AG, the Ontario Ministry of Economic Development and Innovation, Pfizer, the São Paulo Research Foundation (FAPESP) (2013/50724-5), Takeda, and the Wellcome Trust (106169/ZZ14/Z). R.R.R. received financial support from FAPESP (2016/17469-0). We would also like to thank Claire Strain-Damerell and Pavel Savitsky for cloning various mutants of AAK1 and BMP2K proteins that were used in the crystallization trials. Additionally, we thank Dr. Sean Conner for providing the AAK1 plasmids, Dr. Stephane Angers for kindly providing the HEK293T DVL TKO cells, and Dr. Mariann Bienz for providing comments and feedback. We would

like to thank members of the Major laboratory for their feedback and expertise regarding experimental design and project direction.

AUTHOR CONTRIBUTIONS

M.J.A. and M.P.W. co-led molecular characterization of AAK1, designed and carried out molecular biology experiments, and drafted and wrote the manuscript. A.D.A. synthesized SGC-AAK1-1, led the SGC probe declaration effort, and contributed to writing. R.R.R. carried out NanoBRET measurements and cellular IC_{50} measurements. D.S.S. carried out dose-response and pAP2M1 characterization of SGC-AAK1-1 and 25A and contributed to AAK1-LRP6 interaction studies. A.D.R. contributed to cloning and carrying out kinome gain-of-function screen and validation. D.M.G., M.B.R., T.T., and Y.N. aided in AAK1 signaling characterization. M.V.G. developed, generated, and validated LRP5/6 DKO HEK293T cells. J.M.B. carried out the NAK TR-FRET selectivity panel. R.M.C. made AAK1/BMP2K proteins and produced co-crystal structures. D.H.D. proposed and designed analogs. J.M.E. facilitated experimental design and contributed to writing. O.F. facilitated *in vitro* assays. C.G. made AAK1 proteins for crystallization/assays. O.G. facilitated protein synthesis and crystallization. P.H.G. carried out TR-FRET measurements and *in vitro* IC_{50} measurements. N.K. executed compound scale-up for validation studies. S.M. contributed ideas and managed the SGC probe declaration effort. A.S.S. made AAK1/BMP2K proteins for crystallization/assays. F.J.S. made proteins for the NAK selectivity panel and ITC and carried out ITC experiments. C.I.W. synthesized 25A and SGC-AAK1-1N. T.M.W. managed chemistry efforts and aided in the design of molecules. W.J.Z. designed molecules, facilitated SGC probe declaration, and contributed to writing. M.B.M facilitated experimental design, data interpretation, project management, and contributed to writing.

DECLARATION OF INTERESTS

The authors declare no competing interests.

Received: April 25, 2018
Revised: August 27, 2018
Accepted: December 3, 2018
Published: January 2, 2019

REFERENCES

Adams, P.D., Afonine, P.V., Bunkóczi, G., Chen, V.B., Davis, I.W., Echols, N., Headd, J.J., Hung, L.W., Kapral, G.J., Grosse-Kunstleve, R.W., et al. (2010). PHENIX: a comprehensive Python-based system for macromolecular structure solution. Acta Crystallogr. D Biol. Crystallogr. *66*, 213–221.

Anastassiadis, T., Deacon, S.W., Devarajan, K., Ma, H., and Peterson, J.R. (2011). Comprehensive assay of kinase catalytic activity reveals features of kinase inhibitor selectivity. Nat. Biotechnol. *29*, 1039–1045.

Angers, S., and Moon, R.T. (2009). Proximal events in Wnt signal transduction. Nat. Rev. Mol. Cell Biol. *10*, 468–477.

Asquith, C.R.M., Laitinen, T., Bennett, J.M., Godoi, P.H., East, M.P., Tizzard, G.J., Graves, L.M., Johnson, G.L., Dornsife, R.E., Wells, C.I., et al. (2018). Identification and optimization of 4-anilinoquinolines as inhibitors of cyclin G associated kinase. ChemMedChem *13*, 48–66.

Baron, C.B., Pompeo, J., Blackman, D., and Coburn, R.F. (1993). Common phosphatidylinositol 4,5-bisphosphate pools are involved in carbachol and serotonin activation of tracheal smooth muscle. J. Pharmacol. Exp. Ther. *266*, 8–15.

Behrens, J., von Kries, J.P., Kühl, M., Bruhn, L., Wedlich, D., Grosschedl, R., and Birchmeier, W. (1996). Functional interaction of beta-catenin with the transcription factor LEF-1. Nature *382*, 638–642.

Biechele, T.L., Kulikauskas, R.M., Toroni, R.A., Lucero, O.M., Swift, R.D., James, R.G., Robin, N.C., Dawson, D.W., Moon, R.T., and Chien, A.J. (2012). Wnt/β-catenin signaling and AXIN1 regulate apoptosis triggered by inhibition of the mutant kinase BRAFV600E in human melanoma. Sci. Signal. *5*, ra3.

Bilic, J., Huang, Y.L., Davidson, G., Zimmermann, T., Cruciat, C.M., Bienz, M., and Niehrs, C. (2007). Wnt induces LRP6 signalosomes and promotes dishevelled-dependent LRP6 phosphorylation. Science *316*, 1619–1622.

Blitzer, J.T., and Nusse, R. (2006). A critical role for endocytosis in Wnt signaling. BMC Cell Biol. *7*, 28.

Chaikuad, A., Knapp, S., and von Delft, F. (2015). Defined PEG smears as an alternative approach to enhance the search for crystallization conditions and crystal-quality improvement in reduced screens. Acta Crystallogr. D Biol. Crystallogr. *71*, 1627–1639.

Charter, N.W., Kauffman, L., Singh, R., and Eglen, R.M. (2006). A generic, homogenous method for measuring kinase and inhibitor activity via adenosine 5′-diphosphate accumulation. J. Biomol. Screen. *11*, 390–399.

Chen, W.J., Goldstein, J.L., and Brown, M.S. (1990). NPXY, a sequence often found in cytoplasmic tails, is required for coated pit-mediated internalization of the low density lipoprotein receptor. J. Biol. Chem. *265*, 3116–3123.

Chen, V.B., Arendall, W.B., 3rd, Headd, J.J., Keedy, D.A., Immormino, R.M., Kapral, G.J., Murray, L.W., Richardson, J.S., and Richardson, D.C. (2010). MolProbity: all-atom structure validation for macromolecular crystallography. Acta Crystallogr. D Biol. Crystallogr. *66*, 12–21.

Collawn, J.F., Stangel, M., Kuhn, L.A., Esekogwu, V., Jing, S.Q., Trowbridge, I.S., and Tainer, J.A. (1990). Transferrin receptor internalization sequence YXRF implicates a tight turn as the structural recognition motif for endocytosis. Cell *63*, 1061–1072.

Conner, S.D., and Schmid, S.L. (2002). Identification of an adaptor-associated kinase, AAK1, as a regulator of clathrin-mediated endocytosis. J. Cell Biol. *156*, 921–929.

Conner, S.D., Schröter, T., and Schmid, S.L. (2003). AAK1-mediated micro2 phosphorylation is stimulated by assembled clathrin. Traffic *4*, 885–890.

Cowtan, K. (2006). The Buccaneer software for automated model building. 1. Tracing protein chains. Acta Crystallogr. D Biol. Crystallogr. *62*, 1002–1011.

Damke, H., Baba, T., Warnock, D.E., and Schmid, S.L. (1994). Induction of mutant dynamin specifically blocks endocytic coated vesicle formation. J. Cell Biol. *127*, 915–934.

Davis, M.I., Hunt, J.P., Herrgard, S., Ciceri, P., Wodicka, L.M., Pallares, G., Hocker, M., Treiber, D.K., and Zarrinkar, P.P. (2011). Comprehensive analysis of kinase inhibitor selectivity. Nat. Biotechnol. *29*, 1046–1051.

Elkins, J.M., Fedele, V., Szklarz, M., Abdul Azeez, K.R., Salah, E., Mikolajczyk, J., Romanov, S., Sepetov, N., Huang, X.P., Roth, B.L., et al. (2016). Comprehensive characterization of the Published Kinase Inhibitor Set. Nat. Biotechnol. *34*, 95–103.

Emsley, P., Lohkamp, B., Scott, W.G., and Cowtan, K. (2010). Features and development of Coot. Acta Crystallogr. D Biol. Crystallogr. *66*, 486–501.

Gammons, M.V., Renko, M., Johnson, C.M., Rutherford, T.J., and Bienz, M. (2016a). Wnt Signalosome assembly by DEP domain swapping of Dishevelled. Mol. Cell *64*, 92–104.

Gammons, M.V., Rutherford, T.J., Steinhart, Z., Angers, S., and Bienz, M. (2016b). Essential role of the Dishevelled DEP domain in a Wnt-dependent human-cell-based complementation assay. J. Cell Sci. *129*, 3892–3902.

Gupta-Rossi, N., Ortica, S., Meas-Yedid, V., Heuss, S., Moretti, J., Olivo-Marin, J.C., and Israël, A. (2011). The adaptor-associated kinase 1, AAK1, is a positive regulator of the Notch pathway. J. Biol. Chem. *286*, 18720–18730.

Hagemann, A.I., Kurz, J., Kauffeld, S., Chen, Q., Reeves, P.M., Weber, S., Schindler, S., Davidson, G., Kirchhausen, T., and Scholpp, S. (2014). In vivo analysis of formation and endocytosis of the Wnt/β-catenin signaling complex in zebrafish embryos. J. Cell Sci. *127*, 3970–3982.

Hao, H.X., Xie, Y., Zhang, Y., Charlat, O., Oster, E., Avello, M., Lei, H., Mickanin, C., Liu, D., Ruffner, H., et al. (2012). ZNRF3 promotes Wnt receptor turnover in an R-spondin-sensitive manner. Nature *485*, 195–200.

Henderson, D.M., and Conner, S.D. (2007). A novel AAK1 splice variant functions at multiple steps of the endocytic pathway. Mol. Biol. Cell *18*, 2698–2706.

Hernández, A.R., Klein, A.M., and Kirschner, M.W. (2012). Kinetic responses of β-catenin specify the sites of Wnt control. Science *338*, 1337–1340.

Höning, S., Ricotta, D., Krauss, M., Späte, K., Spolaore, B., Motley, A., Robinson, M., Robinson, C., Haucke, V., and Owen, D.J. (2005). Phosphatidylinositol-(4,5)-bisphosphate regulates sorting signal recognition by the clathrin-associated adaptor complex AP2. Mol. Cell *18*, 519–531.

Hu, J., Yuan, Q., Kang, X., Qin, Y., Li, L., Ha, Y., and Wu, D. (2015). Resolution of structure of PIP5K1A reveals molecular mechanism for its regulation by dimerization and dishevelled. Nat. Commun. *6*, 8205.

Huang, Y., Qureshi, I.A., and Chen, H. (1999). Effects of phosphatidylinositol 4,5-bisphosphate and neomycin on phospholipase D: kinetic studies. Mol. Cell. Biochem. *197*, 195–201.

Jiang, Y., He, X., and Howe, P.H. (2012). Disabled-2 (Dab2) inhibits Wnt/β-catenin signalling by binding LRP6 and promoting its internalization through clathrin. EMBO J. *31*, 2336–2349.

Johannessen, C.M., Boehm, J.S., Kim, S.Y., Thomas, S.R., Wardwell, L., Johnson, L.A., Emery, C.M., Stransky, N., Cogdill, A.P., Barretina, J., et al. (2010). COT drives resistance to RAF inhibition through MAP kinase pathway reactivation. Nature *16*, 968–972.

Kabsch, W. (2010). Xds. Acta Crystallogr. D Biol. Crystallogr. *66*, 125–132.

Kadlecova, Z., Spielman, S.J., Loerke, D., Mohanakrishnan, A., Reed, D.K., and Schmid, S.L. (2017). Regulation of clathrin-mediated endocytosis by hierarchical allosteric activation of AP2. J. Cell Biol. *216*, 167–179.

Keller, S., Vargas, C., Zhao, H., Piszczek, G., Brautigam, C.A., and Schuck, P. (2012). High-precision isothermal titration calorimetry with automated peak-shape analysis. Anal. Chem. *84*, 5066–5073.

Kim, I., Pan, W., Jones, S.A., Zhang, Y., Zhuang, X., and Wu, D. (2013). Clathrin and AP2 are required for PtdIns(4,5)P2-mediated formation of LRP6 signalosomes. J. Cell Biol. *200*, 419–428.

Koo, B.K., Spit, M., Jordens, I., Low, T.Y., Stange, D.E., van de Wetering, M., van Es, J.H., Mohammed, S., Heck, A.J., Maurice, M.M., and Clevers, H. (2012). Tumour suppressor RNF43 is a stem-cell E3 ligase that induces endocytosis of Wnt receptors. Nature *488*, 665–669.

Kostich, W., Hamman, B.D., Li, Y.W., Naidu, S., Dandapani, K., Feng, J., Easton, A., Bourin, C., Baker, K., Allen, J., et al. (2016). Inhibition of AAK1 kinase as a novel therapeutic approach to treat neuropathic pain. J. Pharmacol. Exp. Ther. *358*, 371–386.

Kuai, L., Ong, S.E., Madison, J.M., Wang, X., Duvall, J.R., Lewis, T.A., Luce, C.J., Conner, S.D., Pearlman, D.A., Wood, J.L., et al. (2011). AAK1 identified as an inhibitor of neuregulin-1/ErbB4-dependent neurotrophic factor signaling using integrative chemical genomics and proteomics. Chem. Biol. *18*, 891–906.

Lebensohn, A.M., Dubey, R., Neitzel, L.R., Tacchelly-Benites, O., Yang, E., Marceau, C.D., Davis, E.M., Patel, B.B., Bahrami-Nejad, Z., Travaglini, K.J., et al. (2016). Comparative genetic screens in human cells reveal new regulatory mechanisms in WNT signaling. eLife *5*, e21459.

Liberali, P., Snijder, B., and Pelkmans, L. (2014). A hierarchical map of regulatory genetic interactions in membrane trafficking. Cell *157*, 1473–1487.

Liu, C., Kato, Y., Zhang, Z., Do, V.M., Yankner, B.A., and He, X. (1999). beta-Trcp couples beta-catenin phosphorylation-degradation and regulates Xenopus axis formation. Proc. Natl. Acad. Sci. U S A *96*, 6273–6278.

Liu, C., Li, Y., Semenov, M., Han, C., Baeg, G.H., Tan, Y., Zhang, Z., Lin, X., and He, X. (2002). Control of beta-catenin phosphorylation/degradation by a dual-kinase mechanism. Cell *108*, 837–847.

Liu, C.C., Kanekiyo, T., Roth, B., and Bu, G. (2014). Tyrosine-based signal mediates LRP6 receptor endocytosis and desensitization of Wnt/β-catenin pathway signaling. J. Biol. Chem. *289*, 27562–27570.

Madan, B., Walker, M.P., Young, R., Quick, L., Orgel, K.A., Ryan, M., Gupta, P., Henrich, I.C., Ferrer, M., Marine, S., et al. (2016). USP6 oncogene promotes Wnt signaling by deubiquitylating Frizzleds. Proc. Natl. Acad. Sci. U S A *113*, E2945–E2954.

Mao, J., Wang, J., Liu, B., Pan, W., Farr, G.H., 3rd, Flynn, C., Yuan, H., Takada, S., Kimelman, D., Li, L., and Wu, D. (2001). Low-density lipoprotein receptor-related protein-5 binds to Axin and regulates the canonical Wnt signaling pathway. Mol. Cell *7*, 801–809.

McCoy, A.J., Grosse-Kunstleve, R.W., Adams, P.D., Winn, M.D., Storoni, L.C., and Read, R.J. (2007). Phaser crystallographic software. J. Appl. Cryst. *40*, 658–674.

Metcalfe, C., Mendoza-Topaz, C., Mieszczanek, J., and Bienz, M. (2010). Stability elements in the LRP6 cytoplasmic tail confer efficient signalling upon DIX-dependent polymerization. J. Cell Sci. *123*, 1588–1599.

Nusse, R., and Clevers, H. (2017). Wnt/β-catenin signaling, disease, and emerging therapeutic modalities. Cell *169*, 985–999.

Pan, W., Choi, S.C., Wang, H., Qin, Y., Volpicelli-Daley, L., Swan, L., Lucast, L., Khoo, C., Zhang, X., Li, L., et al. (2008). Wnt3a-mediated formation of phosphatidylinositol 4,5-bisphosphate regulates LRP6 phosphorylation. Science *321*, 1350–1353.

Phonphok, Y., and Rosenthal, K.S. (1991). Stabilization of clathrin coated vesicles by amantadine, tromantadine and other hydrophobic amines. FEBS Lett. *281*, 188–190.

Reis, C.R., Chen, P.H., Srinivasan, S., Aguet, F., Mettlen, M., and Schmid, S.L. (2015). Crosstalk between Akt/GSK3β signaling and dynamin-1 regulates clathrin-mediated endocytosis. EMBO J. *34*, 2132–2146.

Ricotta, D., Conner, S.D., Schmid, S.L., von Figura, K., and Honing, S. (2002). Phosphorylation of the AP2 mu subunit by AAK1 mediates high affinity binding to membrane protein sorting signals. J. Cell Biol. *156*, 791–795.

Robers, M.B., Dart, M.L., Woodroofe, C.C., Zimprich, C.A., Kirkland, T.A., Machleidt, T., Kupcho, K.R., Levin, S., Hartnett, J.R., Zimmerman, K., et al. (2015). Target engagement and drug residence time can be observed in living cells with BRET. Nat. Commun. *6*, 10091.

Ruffner, H., Sprunger, J., Charlat, O., Leighton-Davies, J., Grosshans, B., Salathe, A., Zietzling, S., Beck, V., Therier, M., Isken, A., et al. (2012). R-Spondin potentiates Wnt/β-catenin signaling through orphan receptors LGR4 and LGR5. PLoS ONE *7*, e40976.

Schmid, S.L. (2017). Reciprocal regulation of signaling and endocytosis: Implications for the evolving cancer cell. J. Cell Biol. *216*, 2623–2632.

Shi, B., Conner, S.D., and Liu, J. (2014). Dysfunction of endocytic kinase AAK1 in ALS. Int. J. Mol. Sci. *15*, 22918–22932.

Song, B.D., Yarar, D., and Schmid, S.L. (2004). An assembly-incompetent mutant establishes a requirement for dynamin self-assembly in clathrin-mediated endocytosis in vivo. Mol. Biol. Cell *15*, 2243–2252.

Sorrell, F.J., Szklarz, M., Abdul Azeez, K.R., Elkins, J.M., and Knapp, S. (2016). Family-wide structural analysis of human Numb-associated protein kinases. Structure *24*, 401–411.

Taelman, V.F., Dobrowolski, R., Plouhinec, J.L., Fuentealba, L.C., Vorwald, P.P., Gumper, I., Sabatini, D.D., and De Robertis, E.M. (2010). Wnt signaling requires sequestration of glycogen synthase kinase 3 inside multivesicular endosomes. Cell *143*, 1136–1148.

Tamai, K., Semenov, M., Kato, Y., Spokony, R., Liu, C., Katsuyama, Y., Hess, F., Saint-Jeannet, J.P., and He, X. (2000). LDL-receptor-related proteins in Wnt signal transduction. Nature *407*, 530–535.

Toker, A. (1998). The synthesis and cellular roles of phosphatidylinositol 4,5-bisphosphate. Curr. Opin. Cell Biol. *10*, 254–261.

Ultanir, S.K., Hertz, N.T., Li, G., Ge, W.P., Burlingame, A.L., Pleasure, S.J., Shokat, K.M., Jan, L.Y., and Jan, Y.N. (2012). Chemical genetic identification of NDR1/2 kinase substrates AAK1 and Rabin8 Uncovers their roles in dendrite arborization and spine development. Neuron *73*, 1127–1142.

Vasta, J.D., Corona, C.R., Wilkinson, J., Zimprich, C.A., Hartnett, J.R., Ingold, M.R., Zimmerman, K., Machleidt, T., Kirkland, T.A., Huwiler, K.G., et al. (2018). Quantitative, wide-spectrum kinase profiling in live cells for assessing the effect of cellular ATP on target engagement. Cell Chem. Biol. *25*, 206–214.

Walker, M.P., Stopford, C.M., Cederlund, M., Fang, F., Jahn, C., Rabinowitz, A.D., Goldfarb, D., Graham, D.M., Yan, F., Deal, A.M., et al. (2015). FOXP1 potentiates Wnt/β-catenin signaling in diffuse large B cell lymphoma. Sci. Signal. *8*, ra12.

Wang, L.H., Rothberg, K.G., and Anderson, R.G. (1993). Mis-assembly of clathrin lattices on endosomes reveals a regulatory switch for coated pit formation. J. Cell Biol. *123*, 1107–1117.

Winn, M.D., Ballard, C.C., Cowtan, K.D., Dodson, E.J., Emsley, P., Evans, P.R., Keegan, R.M., Krissinel, E.B., Leslie, A.G., McCoy, A., et al. (2011). Overview of the CCP4 suite and current developments. Acta Crystallogr. D Biol. Crystallogr. *67*, 235–242.

Yamamoto, H., Sakane, H., Yamamoto, H., Michiue, T., and Kikuchi, A. (2008). Wnt3a and Dkk1 regulate distinct internalization pathways of LRP6 to tune the activation of beta-catenin signaling. Dev. Cell *15*, 37–48.

Yang, X., Boehm, J.S., Yang, X., Salehi-Ashtiani, K., Hao, T., Shen, Y., Lubonja, R., Thomas, S.R., Alkan, O., Bhimdi, T., et al. (2011).). A public genome-scale lentiviral expression library of human ORFs. Nat. Methods *8*, 659–661.

Yu, A., Rual, J.F., Tamai, K., Harada, Y., Vidal, M., He, X., and Kirchhausen, T. (2007). Association of Dishevelled with the clathrin AP-2 adaptor is required for Frizzled endocytosis and planar cell polarity signaling. Dev. Cell *12*, 129–141.

Zeng, X., Tamai, K., Doble, B., Li, S., Huang, H., Habas, R., Okamura, H., Woodgett, J., and He, X. (2005). A dual-kinase mechanism for Wnt co-receptor phosphorylation and activation. Nature *438*, 873–877.

Zhao, H., Piszczek, G., and Schuck, P. (2015). SEDPHAT—a platform for global ITC analysis and global multi-method analysis of molecular interactions. Methods *76*, 137–148.

STAR★METHODS

KEY RESOURCES TABLE

REAGENT or RESOURCE	SOURCE	IDENTIFIER
Antibodies		
Rabbit polyclonal anti-AAK1	Bethyl Labs	Cat#A302-146A; RRID:AB_1720315
Rabbit monoclonal anti-Clathrin Heavy Chain (D3C6) XP	Cell Signaling Technology	Cat#4796S; RRID:AB_10557412
Rabbit monoclonal anti-LRP6	Cell Signaling Technology	Cat#3395; RRID:AB_1950408
Rabbit polyclonal anti-phospho-LRP6 (S1490)	Cell Signaling Technology	Cat#2568; RRID:AB_2139327
Rabbit polyclonal Anti-Human AP2M1, phospho (Thr156)	Cell Signaling Technology	Cat#3843S; RRID:AB_2056358
Rabbit monoclonal anti-PIP4K2A (D83C1)	Cell Signaling Technology	Cat#5527; RRID:AB_2722636
Rabbit polyclonal anti-Phospho-beta-Catenin (Ser33/37/Thr41)	Cell Signaling Technology	Cat#9561S; RRID:AB_331729
Monoclonal mouse ANTI-FLAG M2	Sigma-Aldrich	Cat#F3165; RRID:AB_259529
Rat monoclonal Anti-HA High Affinity (clone 3F10)	Roche	Cat#11867423001; RRID:AB_390918
Monoclonal mouse anti-beta-Tubulin	Sigma-Aldrich	Cat# T8328; RRID:AB_1844090
Mouse monoclonal anti-LRP6	Abcam	Cat# ab75358; RRID:AB_2139308
Rabbit monoclonal anti-AP2M1 (phospho T156) [EPR4700]	Abcam	Cat# ab109397; RRID:AB_10866362
Rabbit monoclonal anti-AP2M1 [EP2695Y]	Abcam	Cat# ab75995; RRID:AB_1309955
Mouse monoclonal anti-CTNNB1	BD Biosciences	Cat#163510
Mouse monoclonal anti-GSK-3 beta	BD Biosciences	Cat#610201; RRID:AB_397600
Mouse monoclonal anti-Dvl-3	Santa Cruz Biotechnology	Cat# sc-8027; RRID:AB_627434
Mouse monoclonal beta-actin	Santa Cruz Biotechnology	Cat# sc-47778 HRP; RRID:AB_2714189
Rabbit polyclonal AP2M1	Thermo Fisher Scientific	Cat# PA5-21360; RRID:AB_11154082
IRDye 800CW Goat anti Mouse IgG	LI-COR Biosciences	Cat# P/N 925-32210; RRID:AB_2687825
IRDye 680LT Goat anti Mouse IgG	LI-COR Biosciences	Cat#P/N 925-68020; RRID:AB_2687826
IRDye800CW Goat anti Rabbit IgG	LI-COR Biosciences	Cat#925-32211; RRID:AB_2651127
IRDye 680LT Goat anti Rabbit IgG	LI-COR Biosciences	Cat#P/N 925-68021; RRID:AB_2713919
Mouse monoclonal anti-LRP6 (Clone 255302)	R and D Systems	Cat# MAB1505; RRID:AB_10889810
Monoclonal mouse IgG2A Isotype Control (Clone 20102)	R and D Systems	Cat# MAB003; RRID:AB_357345
R-Phycoerythrin-AffiniPure F(ab')2 Fragment Goat Anti-Mouse IgG	Jackson Immunoresearch	Cat#115-116-146; RRID:AB_2338629
Polyclonal rabbit anti-GFP	Abcam	Cat# ab290; RRID:AB_303395
Bacterial and Virus Strains		
BL21(DE3) for recombinant protein expression	Laboratory of Dr. Opher Gileadi	N/A
Chemicals, Peptides, and Recombinant Proteins		
CHIR99021	Cayman Chemicals	Cat#13122 ; Cas#252917-06-9
Chlorpromazine HCL	Sigma-Aldrich	Cat#C0982 ; Cas#69-09-0
Bafilomycin A1	Cayman Chemicals	Cat#11038 ; Cas#88899-55-2
WNT3A	PeproTech	Cat#315-20
WNT5A	R and D Systems	Cat#645-WN-010
Neomycin trisulfate salt hydrate	Sigma-Aldrich	Cat#N6386 ; Cas#1405-10-3
Carbachol	EMD Chemicals	Cat#212385 ; Cas#51-83-2
Staurosporine	Sigma-Aldrich	Cat#S4400; Cas# 62996-74-1
NanoBRET Tracer K-5	Promega	Cat# N248A
AP-2 derived peptide	WatsonBio	Custom (biotin-GGSQITSQVTGQIGWRR-amide)

(*Continued on next page*)

Continued

REAGENT or RESOURCE	SOURCE	IDENTIFIER
Critical Commercial Assays		
Pierce Cell Surface Protein Isolation Kit	ThermoFisher	Cat#89881
PureLink RNA Mini Kit	Invitrogen	Cat#12183018A
iScript cDNA Synthesis Kit	BioRad	Cat#1708891
Dual-Luciferase Reporter Assay System	Promega	Cat#E1910
Deposited Data		
Gain-of-function kinome screen	This paper	Mendeley Data: https://doi.org/10.17632/352fxh8r6t.1 ; https://doi.org/10.17632/352fxh8r6t.1#file-94081320-ab20-4178-8be2-233c7ea23b62
KINOMEscan	This paper	Mendeley Data: https://doi.org/10.17632/cz9bx7d52c.1 ; https://data.mendeley.com/datasets/cz9bx7d52c/draft/files/bd678698-6718-4979-8b9e-1b0f7645884e/KINOMEscan%20Results%20for%20AAK1.xlsx?dl=1
BMP2K K_D bound to 25A	This paper	PDB ID: 5IKW ; https://www.rcsb.org/structure/5IKW
Experimental Models: Cell Lines		
Human male: HT1080	ATCC	CCL-121
Human fetus: HEK293T/17	ATCC	CRL-11268
Human: RKO	ATCC	CRL-2577
Mouse male: Lcells	ATCC	CRL-2648
Mouse male: WNT3A expressing Lcells	ATCC	CRL-2647
Oligonucleotides		
See Table S7 for complete list		N/A
Recombinant DNA		
Human kinase open reading frame library	Yang et al., 2011 ; Johannessen et al., 2010	Addgene #1000000014
Flag-AAK1-WT	Dr. Sean Conner	Conner et al., 2003
Flag-AAK1-dAID	Dr. Sean Conner	Conner et al., 2003
Flag-AAK1-74A	Dr. Sean Conner	Conner et al., 2003
GFP-LRP6	Dr. Randell Moon	This paper
HA-LRP6	Dr. Randell Moon	This paper
ANKRD6	Dr. Randell Moon	This paper
FLAG-dnTCF7L2	Dr. Randell Moon	Walker et al., 2015.
TK-*Renilla*	Dr. Randell Moon	Walker et al., 2015.
BAR-reporter	Dr. Randell Moon	Walker et al., 2015.
NFκB-reporter		Walker et al., 2015.
TGFβ-reporter		Walker et al., 2015.
ADCK1	Yang et al., 2011 ; Johannessen et al., 2010	Addgene #1000000014
ADCK2	Yang et al., 2011 ; Johannessen et al., 2010	Addgene #1000000014
MAST1	Yang et al., 2011 ; Johannessen et al., 2010	Addgene #1000000014
TGFBR3	Yang et al., 2011 ; Johannessen et al., 2010	Addgene #1000000014
K44A Dynamin 1 pEGFP	Song et al., 2004	Addgene #34681

(*Continued on next page*)

Continued

REAGENT or RESOURCE	SOURCE	IDENTIFIER
Software and Algorithms		
Design-Expert software	Stat-Ease, version 10	https://www.statease.com/
SEDPHAT	Zhao et al., 2015	sedfitsedphat.nibib.nih.gov
NITPIC	Keller et al., 2012	http://biophysics.swmed.edu/MBR/software.html
TREEspot	DiscoverX	https://www.discoverx.com/services/drug-discovery-development-services/treespot-data-analysis
Other		
Streptavidin beads	GE Healthcare	Cat#17-5113-01
Protein A/G Agarose	ThermoFisher	Cat#20421
EZview Red Flag M2 Affinity Gel	Sigma-Aldrich	Cat#F2426
EZview Red Anti-HA Affinity Gel	Sigma-Aldrich	Cat#E6779
NuPAGE 4-12% Bis-Tris Protein Gels	ThermoFisher	Cat#NP0321BOX
Nitrocellulose Membrane	ThermoFisher	Cat#88018
TansIT2020	Mirus Bio	Cat#MIR5405
RNAiMAX	Life technologies	Cat#13778030
Fast SYBER Green Master Mix	Applied Biosystems	Cat#4385612
NanoLuc-AAK1 fusion vector	Promega	Cat#NV1001
NanoLuc-BMP2K fusion vector	Promega	Cat#NV1091

CONTACT AND REAGENT RESOURCE SHARING

Further information and requests for resources and reagents should be directed to and will be fulfilled by the Lead Contact, Michael B. Major (ben_major@email.unc.edu).

EXPERIMENTAL MODEL AND SUBJECT DETAILS

Cell lines and tissue culture

All cells were cultured at 37°C and 5% CO_2. HT1080 (human male), HEK293T/17 (human fetus), RKO (human, gender N/A), Lcells (mouse male), and WNT3A expressing Lcells (mouse male) were obtained from American Type Culture Collection (ATCC, Manassas, VA) and grown in DMEM with 10% FBS. Each cell line was tested for mycoplasma contamination and passaged no more than 20 passages from the original ATCC stock. Cells were treated at the indicated concentrations with the following compounds: CHIR99021 (Cayman Chemicals, Ann Arbor, MI), chlorpromazine HCL (Sigma-Aldrich, St. Louis, MO), bafilomycin A1 (Cayman Chemicals), rhWNT3A (PeproTech, Rocky Hill, NJ), rhWNT5A (R&D, Minneapolis, MN), neomycin trisulfate salt hydrate (Sigma-Aldrich) and carbachol (EMD Chemicals, Gibbstown, NJ).

METHOD DETAILS

WNT3A conditioned media

Conditioned media was collected as described by ATCC. Briefly, WNT3A and control Lcells were grown to 100% confluency before fresh media was added, conditioned for 48 hr, and then collected.

Immunoprecipitation and immunoblotting

Immunoprecipitation (IP) experiments were performed as previously described (Jiang et al., 2012). Briefly, cells were lysed in 1% Triton lysis buffer, passed through an 18 gauge needle, and cleared via centrifugation at max speed for 10 mins. For endogenous IP experiments, antibody was conjugated to activated Protein A/G beads (ThermoFisher) for 1 hr at 4°C with nutation. Conjugated beads were then added to cleared lysate and incubated for 4 hr at 4°C with nutation. For overexpression IP experiments, activated Flag (Sigma-Aldrich) or HA (Sigma-Aldrich) beads were added directly to the cleared lysate and incubated for 1 hr at 4°C with nutation. Following incubation, beads were washed 5 times with lysis buffer, then the sample was eluted at 95°C for 5 mins, and a W.blot was performed. Standard W.blotting techniques were utilized. Briefly, samples were run on a NuPAGE 4%–12% Bis-Tris Protein Gel (ThermoFisher), then transferred to a nitrocellulose membrane. The membrane was then blocked and incubated overnight with primary antibody at 4°C with rotation, washed with TBST, incubated with secondary antibody, washed with TBST and imaged.

All images were obtained using a LiCOR Odyssey imager and quantified with LiCOR software. For W.blot analysis, all antibodies were used at a concentration of 1:1000, with the exception of loading controls, which were used at 1:10,000. Bethyl Labs (Montgomery, TX) – AAK1 (A302-146a); Cell Signaling (Danvers, MA) – Clathrin (4796), LRP6 (3395), phospho-LRP6 (S1490) (2568), phospho-AP2M1 (T156) (7399S), PIP4K2A (5527), phospho-CTNNB1 (S33/37/T41) (9561S); Sigma-Aldrich – FLAG M2 (F3165), HA (11867423001), and beta-tubulin (T8328); Abcam (Cambridge, UK) – LRP6 (ab75358), AP2M1 (ab7995), p-AP2M1 (Thr156) (ab109397); BD Biosciences (San Jose, CA) – CTNNB1 (610153), GSK3β (610201); Santa Cruz (Dallas, TX) – DVL3 (sc-8027), beta-actin (sc-47778); Invitrogen (Carlsbad, CA) - AP2M1 (PA5-21360). Secondary antibodies were used at 1:5000 dilution and purchased from LiCOR Biosciences. Specific antibodies used are as follows: IRDye® 800CW Goat anti Mouse IgG (925-32210), IRDye® 680LT Goat anti Mouse IgG (925-68020), IRDye®800CW Goat anti Rabbit IgG (925-32211), and IRDye® 680LT Goat anti Rabbit IgG (925-68021).

Surface staining of LRP6

HEK293T cell were transfected for 48 hr prior to splitting into 60 cm plates with 400,000 cells/plate and allowed to attach overnight. Cells were disassociated with 0.5 mM EDTA in DPBS and washed with FACS Buffer (2% FBS in DPBS). Cells were stained in FACS buffer for 1 hour at on ice using 5 μg/mL LRP6 antibody (R&D) or Isotype Control (R&D) and secondary staining with 1:100 anti-mouse PE (Jackson Immunoresearch, West Grove, PA) for 45 mins. After staining, cells were fixed with 2% paraformaldehyde in FACS buffer and analyzed by the UNC-Flow Cytometry Core.

DNA constructs and siRNAs

The human kinase open reading frame library was obtained from Addgene (cat# 1000000014) and cloned into a custom pHAGE-CMV-FLAG vector using Gateway cloning technology. All constructs were N-terminally sequence verified. Gain-of-function kinome screen data is presented in Table S3 and has been deposited on Mendeley Data (https://doi.org/10.17632/352fxh8r6t.1#file-94081320-ab20-4178-8be2-233c7ea23b62). Wild-type AAK1 and mutants were a gift from Dr. Sean Conner (University of Minnesota). GFP-LRP6, HA-LRP6, ANKRD6, and FLAG-dnTCF7L2 were kindly provided by Dr. Randell Moon (University of Washington). ADCK1, ADCK2, MAST1, and TGFBR3 were obtained as part of the kinome library from Addgene. GFP-Dynamin1-K44A was obtained from Addgene. All siRNAs were obtained from Life Technologies (ThermoFisher, Waltham, MA), and sequences are listed in Table S7.

Transcriptional reporter assays

All luciferase reporter assays and IncuCyte fluorescent reporter assays were performed as previously described (Walker et al., 2015). Briefly, for loss-of-function assays, cell lines stably expressing the BAR-Firefly luciferase reporter and TK-*Ren* luciferase were used and transfected with RNAiMAX (Life technologies, ThermoFisher) for 72 hr. For gain of function studies, the BAR-reporter (20 ng), TK-*Ren* (10 ng), and indicated constructs (70 ng) were transfected with TansIT2020 (Mirus Bio) for 24 hr. For IncuCyte fluorescent reporter assays, stable BAR-mCherry cells were treated and imaged as indicated using the IncuCyte Live Cell Analysis System from Essen BioScience. Luciferase readouts were normalized using co-transfected TK-*Ren* (Luciferase assays) and IncuCyte Analysis was normalized to internal mCherry control. Conditions were plated in triplicate, and normalized values were averaged across triplicates to yield the data presented and standard error. Each assay was repeated in biological triplicate, unless otherwise stated. Firefly luciferase and the *Renilla (Ren)* control were detected using the Promega Dual-Luciferase Reporter Assay System per the manufacturer's protocol (Promega, Madison, WI). Plates were read on the EnSpire plate reader from PerkinElmer.

Real-Time Quantitative PCR

Quantitative PCR (qPCR) was performed as described previously (Walker et al., 2015). Briefly, cells were treated as indicated and RNA was collected using PureLink RNA Mini Kit (Invitrogen, Carlsbad, CA). cDNA was generated from 1ug of RNA using the iScript cDNA Synthesis Kit (BioRad, Hercules, CA) following kit specifications. qPCR was performed using Fast SYBER Green Master Mix (Applied Biosystems, Foster City, CA) on the Applied Biosystems 7400HT following manufacturer specifications. Samples were run in technical triplicate on a 384-well plate, with biological triplicates run on subsequent plates. Primers were previously published (Walker et al., 2015) and sequences are listed in Table S7.

Generation of LRP5/6 DKO stable cell lines

HEK293T cells were transfected with Cas9 and sgRNAs targeting LRP5/6. Sequences are listed in Table S7. Deletions were confirmed by immunoblotting and verified via sequencing.

Surface biotinylation

For surface biotinylation assays, the Pierce Cell Surface Protein Isolation Kit (ThermoFisher) was utilized and manufacturer specifications were followed. Briefly, cells were grown to 70% confluency, washed 3 times with cold PBS, and then biotinylated for 30 mins at 4°C with NHS-SS-sulfo-linked biotin (0.25mg/mL). The free biotin was quenched, and then the samples were washed 3 times with cold TBS prior to lysis and sonication. Lysates were cleared and then incubated with Streptavidin beads (GE Healthcare, Little Chalfont, UK) for 1 hour at 4°C with nutation. Beads were washed 4 times with cold TBS and then proteins were eluted with LDS protein loading buffer supplemented with DTT at 95°C for 10 mins.

Chemistry general procedures

Reagents were purchased from commercial suppliers and used without further purification. ^{1}H and ^{13}C NMR spectra were collected in methanol-d_4 and recorded on Varian Inova 400 or Inova 500 spectrometers. Peak positions are given in parts per million (ppm) downfield from tetramethylsilane as the internal standard; J values are expressed in hertz. Thin-layer chromatography (TLC) was performed on silica gel F254 to evaluate reaction courses and mixtures. Flash chromatography was performed on Merck 60 silica gel (0.063–0.200 mm). All non-aqueous reactions were performed under nitrogen atmosphere. Solutions containing the final products were dried over Na_2SO_4 before filtration and concentration under reduced pressure using a rotary evaporator.

Crystal structure determination

Diffraction data were integrated using XDS (Kabsch, 2010) and scaled using AIMLESS from the CCP4 software suite (Winn et al., 2011). Molecular replacement was performed with Phaser (McCoy et al., 2007) using BMP2K/AZD7762 (PDB: 4W9W) (Sorrell et al., 2016) as a search model. Automated model building was performed with Buccaneer (Cowtan, 2006). Automated refinement was performed in PHENIX (Adams et al., 2010). Coot (Emsley et al., 2010) was used for manual model building and real space refinement. Structure validation was performed using MolProbity (Chen et al., 2010). Structure factors and coordinates have been deposited in the PDB with code 5IKW.

Binding-displacement assays

The TR-FRET ligand binding-displacement assays for AAK1, BMP2K, GAK and STK16 were performed as previously described (Asquith et al., 2018). Inhibitor binding was determined using a binding-displacement assay, which measures the ability of inhibitors to displace a fluorescent tracer compound from the ATP binding site of the kinase domain. Inhibitors were dissolved in DMSO and dispensed as 16-point, 2x serial dilutions in duplicate into black multi-well plates (Greiner). Each well contained either 0.5 nM or 1 nM biotinylated kinase domain protein ligated to streptavidin-Tb-cryptate (Cisbio), 12.5 nM or 25 nM Kinase Tracer 236 (ThermoFisher Scientific), 10 mM HEPES pH 7.5, 150 mM NaCl, 2 mM DTT, 0.01% BSA, 0.01% Tween-20. Final assay volume for each data point was 5 μL, and final DMSO concentration was 1%. The kinase domain proteins were expressed in *E. coli* as a fusion with a C-terminal AVI tag (vector pNIC-Bio3, NCBI reference JN792439) which was biotinylated by co-expressed BirA, and purified using the same methods as used previously (Asquith et al., 2018). After setting up the assay plate it was incubated at room temperature for 1.5 hours and then read using a TR-FRET proto Residue ranges were AAK1: 31-396, BMP2K: 38-345, GAK: 12-347, STK16: 13-305col on a PheraStarFS plate reader (BMG Labtech). The data was normalized to 0% and 100% inhibition control values and fitted to a four parameter dose-response binding curve in GraphPad Software (version 7, La Jolla, CA, USA). The determined IC_{50} values were converted to Ki values using the Cheng-Prusoff equation and the concentration and K_D values for the tracer (previously determined).

Kinome screening

The KINOMEscan assay panel was measured at DiscoverX Corporation as previously described (Davis et al., 2011). Data collection can be found in Table S2 and has been deposited on Mendeley Data (https://doi.org/10.17632/cz9bx7d52c.1#file-bd678698-6718-4979-8b9e-1b0f7645884e). Kinases were produced either as fusions to T7 phage3, or were expressed as fusions to NF-κB in HEK293 cells and subsequently tagged with DNA for PCR detection18. In general, full-length constructs were used for small, single-domain kinases, and catalytic domain constructs including appropriate flanking sequences were used for multidomain kinases. Briefly, for the binding assays, streptavidin-coated magnetic beads were treated with biotinylated affinity ligands to generate affinity resins. The liganded beads were blocked to reduce nonspecific binding and washed to remove unbound ligand. Binding reactions were assembled by combining kinase, liganded affinity beads and test compounds prepared as 100 × stocks in DMSO. DMSO was added to control assays lacking a test compound. Primary screen interactions were performed in 384-well plates, whereas K_D determinations were performed in 96-well plates. Assay plates were incubated at 25°C with shaking for 1 h, and the affinity beads were washed extensively to remove unbound protein. Bound kinase was eluted in the presence of non-biotinylated affinity ligands for 30 min at 25°C with shaking. The kinase concentration in the eluates was measured by quantitative PCR. K_D values were determined using 11 serial threefold dilutions of test compound and a DMSO control.

N-(6-(3-((N,N-diethylsulfamoyl)amino)phenyl)-1H-indazol-3-yl)cyclopropanecarboxamide (SGC-AAK1-1)

3-Aminophenylboronic acid pinacol ester (1 eq., 50 mg, 0.228 mmol) in pyridine (1.2 mL) was cooled to 0°C in an ice bath. Diethylsulfamoyl chloride (2.06 eq., 80.7 mg, 0.0754 mL, 0.47 mmol) was added drop wise, and the reaction mixture was stirred overnight. The reaction progress was checked by TLC, revealing complete consumption of starting material (SM). Solvent was removed and the residue was partitioned between dichloromethane and saturated aqueous sodium bicarbonate solution. The organic phase was dried (Na_2SO_4), filtered and concentrated. The residue was purified using an Isco Combiflash companion automated purification system (4g (18 mL/min), SiO_2, 80%/20% to 25%/75% heptanes/EtOAc) to give diethyl({[3-(tetramethyl-1,3,2-dioxaborolan-2-yl)phenyl]sulfamoyl})amine as an orange solid (44 mg, 54%), which was determined to be desired product by ^{1}H NMR.

The following was added to a microwave vial: N-(6-bromo-1H-indazol-3-yl)cyclopropanecarboxamide (1 eq., 20 mg, 0.0677 mmol), diethyl({[3-(tetramethyl-1,3,2-dioxaborolan-2-yl)phenyl]sulfamoyl})amine (1 eq., 24 mg, 0.0677 mmol), and Pd(dppf)Cl2 (10%, 4.96 mg, 0.00677 mmol) in a mixture of dioxane (0.19 mL) and 1M aq sodium carbonate (0.16 mL). The vial was capped and heated in the microwave at 120°C for 30 mins. Once cool, the reaction progress was examined by TLC, which revealed complete

consumption of SM. The mixture was filtered through Celite and washed with EtOAc (ethyl acetate). The combined organic solution was washed with brine, dried (Na_2SO_4), filtered and concentrated. The residue was purified using an Isco Combiflash companion automated purification system (4g (18 mL/min), SiO_2, 75%/25% to 20%/80% heptanes/EtOAc) to give **SGC-AAK1-1** as a yellow solid (14.3 mg, 49%): ^{1}H NMR (400 MHz, Methanol-d_4) δ 7.80 (d, J = 0.8 Hz, 1H), 7.58 (s, 1H), 7.48 (dt, J = 0.8, 2.1 Hz, 1H), 7.38 – 7.35 (m, 2H), 7.33 (d, J = 8.5 Hz, 1H), 7.17 – 7.12 (m, 1H), 3.29 (d, J = 1.6 Hz, 4H), 1.91 (tt, J = 4.5, 8.0 Hz, 1H), 1.05 (t, J = 7.1 Hz, 6H), 1.01 (dt, J = 3.0, 4.4 Hz, 2H), 0.95 – 0.88 (m, 2H); ^{13}C NMR (101 MHz, Methanol-d_4) δ 174.1, 142.1, 141.9, 139.8, 139.0, 129.1, 122.2, 121.6, 119.7, 118.3, 118.1, 107.5, 48.2, 41.6, 13.5, 12.5, 6.8.

General procedure for preparation of 3-acylamino-6-bromoindazoles

To a solution of 6-bromo-1H-indazol-3-amine (48 mg, 0.23 mmol) in pyridine (0.75 mL) was added cyclopropanecarboxylic acid chloride (0.021 mL, 0.23 mmol, 1 eq.,) drop wise at 0 °C. The reaction mixture was stirred at this temperature for 4 hr and then allowed to warm to room temperature. Once the reaction was complete the solvent was removed under reduced pressure. The residue was then dissolved in N,N-dimethylformamide and water was added drop wise. The precipitated solid was then washed with hexanes 3 times and further dried to afford *N*-(6-bromo-1*H*-indazol-3-yl)cyclopropanecarboxamide (40.4 mg, 64% yield).

General procedure for 3-acylamino-6-arylindazoles

The following was added to a microwave vial: *N*-(6-bromo-1H-indazol-3-yl)cyclopropanecarboxamide (344 mg, 1.12 mmol) dissolved in dioxane (4mL) and 1M Na_2CO_3 (1mL). To this solution, the following was added: 3-aminophenylboronic acid pinacol ester (269 mg, 1.12 mmol, 1.0 eq.,), Pd(dppf)Cl_2 (100.3 mg, 0.123 mmol, 0.1eq,). The reaction was run in the microwave at 160 °C for 20 mins, at which time SM was consumed. The reaction mixture was poured into water and extracted 3 times with EtOAc. The combined organic layers were dried over Na_2SO_4 and concentrated to dryness. The compound was then purified by flash chromatography to afford *N*-(6-(3-aminophenyl)-1*H*-indazol-3-yl)cyclopropanecarboxamide (100 mg, 28% yield).

N-(6-(3-(cyclopropanesulfonamido)phenyl)-1H-indazol-3-yl)cyclopropanecarboxamide (25A)

To a solution of *N*-[6-(3-aminophenyl)-1H-indazol-3-yl]cyclopropanecarboxamide (67mg, 0.2292 mmol) in pyridine (1mL) cooled to 0 °C, cyclopropanesulfonyl chloride (1eq, 32.22mg, 0.2292 mmol) was added drop wise. The reaction mixture was stirred at 0 °C for 4 hr and warmed to room temperature. After verification by LC/MS that SM had been consumed, solvent was removed under reduced pressure. The compound was then purified by high pressure liquid chromatography (HPLC) from 10% to 100% ACN/water + 0.05% TFA to yield **25A** (44.5 mg, 49% yield). ^{1}H NMR (400 MHz, Methanol-d_4) δ 7.83 – 7.78 (d, J = 8.6 Hz, 1H), 7.61 – 7.54 (m, 2H), 7.46 – 7.30 (m, 3H), 7.29 – 7.23 (ddd, J = 7.7, 2.2, 1.3 Hz, 1H), 2.62 – 2.49 (tt, J = 8.0, 4.8 Hz, 1H), 1.95 – 1.84 (ddd, J = 12.5, 7.9, 4.2 Hz, 1H), 1.07 – 0.77 (m, 8H). ^{13}C NMR (126 MHz, Methanol-d_4) δ 5.8 (2C), 8.4 (2C), 15.0, 30.5, 30.8, 109.1, 117.2, 121.2, 121.3, 121.4, 123.1, 124.7, 130.8, 140.1, 141.2, 143.4 (2C), 143.8, 175.6. MS+ (– ES API) - 397.1.

N-(6-(3-(cyclopropanesulfonamido)phenyl)-1H-indazol-3-yl)isobutyramide (SGC-AAK-1N):

^{1}H NMR (400 MHz, Methanol-d_4) δ 7.82 – 7.75 (d, J = 8.6 Hz, 1H), 7.62 – 7.54 (dt, J = 10.9, 1.5 Hz, 2H), 7.47 – 7.31 (m, 3H), 7.31 – 7.22 (ddd, J = 7.8, 2.2, 1.3 Hz, 1H), 2.84 – 2.69 (hept, J = 6.8 Hz, 1H), 2.61 – 2.50 (tt, J = 8.0, 4.8 Hz, 1H), 1.29 – 1.15 (d, J = 6.8 Hz, 6H), 1.14 – 0.82 (m, 4H). ^{13}C NMR (126 MHz, Methanol-d_4) δ 5.8 (2C), 20.0 (2C), 30.5, 36.3, 109.2, 117.4, 121.3, 121.4 (2C), 123.0, 124.7, 130.8, 140.1, 141.2, 141.3, 143.4, 143.8, 179.3. MS+ (– ES API) - 399.1.

Cloning, protein expression and purification

For crystallization of BMP2K, a construct of BMP2K residues 38-345 (NCBI NP_942595) encompassing the kinase domain with surface mutations K320A and K321A in expression vector pNIC-Zb was used (Sorrell et al., 2016). The construct was transformed into BL21(DE3) cells that co-express λ-phosphatase and three rare tRNAs (plasmid pACYC-LIC+). The cells were cultured in TB medium containing 50 μg/mL kanamycin and 35 μg/mL chloramphenicol at 37°C with shaking until the OD600 reached ~3 and then cooled to 18°C for 1 hour. Isopropyl β-D-1-thiogalactopyranoside (IPTG) was added to a final concentration of 0.1 mM and the cultures were left overnight at 18°C. The cells were collected by centrifugation then resuspended in 2x lysis buffer (100 mM HEPES buffer, pH 7.5, 1.0 M NaCl, 20 mM imidazole, 1.0 mM tris(2-carboxyethyl)phosphine (TCEP), Protease Inhibitor Cocktail Set VII (Calbiochem, 1/500 dilution) and flash-frozen in liquid nitrogen. Cells were lysed by sonication on ice. The resulting proteins were purified using Ni-Sepharose resin (GE Healthcare) and eluted stepwise in binding buffer with 300 mM imidazole. Removal of the hexahistidine tag was performed at 4°C overnight using recombinant TEV protease. Protein was further purified using reverse affinity chromatography on Ni-Sepharose followed by gel filtration (Superdex 200 16/60, GE Healthcare). Protein in gel filtration buffer (25 mM HEPES, 500 mM NaCl, 0.5 mM TCEP, 5% [v/v] glycerol) was concentrated to 12 mg/mL (measured by UV absorbance, using the calculated molecular weight and estimated extinction coefficient, using a NanoDrop spectrophotometer (Thermo Scientific) using 30 kDa molecular weight cut-off centrifugal concentrators (Millipore) at 4°C.

NanoBRET measurements

Constructs for NanoBRET measurements of AAK1 and BMP2K were kindly provided by Promega. The AAK1 construct represents the short isoform of AAK1 with an N-terminal Nanoluc fusion, and the BMP2K construct represents residues the short isoform of BMP2K with an N-terminal Nanoluc fusion. HEK293T cells (ATCC) were maintained in DMEM supplemented with 10% fetal bovine serum (FBS) (Life Technologies) with penicillin and streptomycin. NanoLuc-AAK1 or NanoLuc-BMP2K fusion constructs were complexed with Lipofectamine 2000 according to the manufacturer's protocol (Invitrogen). DNA:Lipofectamine complexes were formed with 24 μg DNA and 60 μL Lipofectamine. The transfection complexes were then mixed with HEK293T cells in a 100 mm dish at 50%–70% confluence in serum-free DMEM (Lonza), followed by incubation in a humidified, 37°C, 5% CO2 incubator. After 4 hr of incubation, the medium was replaced by 10% FBS DMEM with antibiotics and the cells were incubated for an additional 20 hr. The NanoBRET assay was performed as previously described (Robers et al., 2015). Briefly, cells were trypsinized and resuspended in Opti-MEM without phenol red (Life Technologies). Cells (85 μL) were then seeded into white, nonbinding surface plates (Corning) at a density of 2×10^4 cells/well. Diluted tracer was prepared from 200 μM stock in Tracer Dilution Buffer (32.25% PEG400 in 12.5 mM HEPES Buffer pH 7.5) at a 1 to 4 ratio, and 5 μL was added to the cells to have a final concentration of 2, 1, 0.5 or 0.25 μM. All chemical inhibitors were prepared as concentrated stock solutions in dimethylsulfoxide (DMSO) (Sigma-Aldrich). Serial dilutions of the inhibitors at 50x the final assay concentration were made by dilution with DMSO, before the inhibitors were added to the cells at 1:50 ratio (2% final DMSO concentration). Cells were then incubated for 2 hr before Bioluminescence resonance energy transfer (BRET) measurements. To measure BRET, NanoBRET NanoGlo Substrate (Promega) was added, and filtered luminescence was measure on a BMG LABTECH Clariostar luminometer equipped with 450 nm BP filter (donor) and 610 nm LP filter (acceptor), using 0.5 s integration time with gain settings of 3,600 for both filters. Background-corrected BRET ratios were determined by subtracting the BRET ratios of samples with no tracer added.

Measurement of *in vitro* IC_{50} values for inhibition of AAK1 enzymatic activity

Enzymatic activity of AAK1 was monitored in 20 μL reaction volumes containing 25 nM AAK1 (27-365) in 15 mM MOPS pH 7.5, 2 mM $MgCl_2$ and 0.004% Triton X-100 buffer plus 46 μM ATP (at K_m) and 200 μM of an AP-2 derived peptide (biotin-GGSQITSQVTG QIGWRR-amide). Optimal activity was achieved with sample incubation at 37°C for 40 mins (steady-state conditions) in buffer conditions that were tailored by factorial design using Design-Expert software (Stat-Ease, version 10). To generate inhibition curves, end-point reactions were setup having compounds pre-incubated in a reaction mix without ATP for 10 mins at room temperature. Next, all samples (in PCR tubes) were transferred to a PCR instrument set at 37°C for another 5 mins. The reaction started with the addition of 46 μM ATP (at K_m), maintaining the incubation conditions for another 40 mins. The reactions were stopped and the amount of ADP produced was measured using a coupled enzyme assay system that converts Amplex Red to Resorufin (Charter et al., 2006). Fluorescence readings were made in a BMG Labtech Clariostar instrument with excitation peak set at 530 nm and emission peak reading at 590 nm.

Protein crystallization

The AAK1 inhibitor (dissolved in 100% DMSO) was added to the protein in a 3-fold molar excess and incubated on ice for approximately 30 mins. The mixture was centrifuged at 14,000 rpm for 10 mins at 4°C prior to setting up 150 nL volume sitting drops at three ratios (2:1, 1:1, or 1:2 protein-inhibitor complex to reservoir solution). Crystallization experiments were performed at 20°C. Crystals were cryoprotected in mother liquor supplemented with 20%–25% glycerol before flash-freezing in liquid nitrogen for data collection. Diffraction data was collected at the Diamond Light Source. The best diffracting crystals grew in 10% (v/v) Broad MW PEG smear, 3.2 M $MgCl_2$, 100 mM HEPES pH 7.0 (Chaikuad et al., 2015). Data was collected at 100 K at the Diamond Synchrotron beamline I02. Data collection statistics can be found in Table S5.

Isothermal Titration Calorimetry

AAK1 and BMP2K proteins were produced as previously described (Sorrell et al., 2016). Isothermal titration calorimetry measurements were made on a Microcal VP-ITC instrument at 25°C. For the interaction of AAK1 with SGC-AAK1-1, the compound was diluted to 22 μM in ITC buffer from a stock at 10 mM in DMSO and loaded directly into the cell. AAK1 was dialyzed at 4°C overnight into ITC buffer (20 mM HEPES pH 7.5, 150 mM NaCl, 1 mM TCEP) and loaded into the ITC syringe at a final concentration of 218 μM. Following thermal equilibration, AAK1 was titrated into the cell using serial injections of 8 μL until saturation was observed in the thermogram. The same method was repeated for the BMP2K versus SGC-AAK1-1 interaction where protein was loaded into the syringe at a concentration of 288 μM and injected into a 32 μM solution of SGC-AAK1-1. The ITC data was analyzed with NITPIC (Keller et al., 2012) and SEDPHAT (Zhao et al., 2015). The final fitted data values are in Table S4.

QUANTIFICATION AND STATISTICAL ANALYSIS

Statistics

All error bars are ± standard error (SE). Statistical significance was evaluated by Mann-Whitney t test unless otherwise stated. N values are stated in figure legends. Each panel was performed in at least biological triplicate, with higher replicates noted in figure legend. *** $p < 0.0005$, ** $p < 0.005$, * $p < 0.05$.

DATA AND SOFTWARE AVAILABILITY

Gain-of-function kinome screen

The reference number for the gain-of-function kinome screen reported in this paper is Mendeley Data (https://doi.org/10.17632/352fxh8r6t.1).

KINOMEscan

The reference number for the KINOMEscan reported in this paper is Mendeley Data (https://doi.org/10.17632/cz9bx7d52c.1).

BMP2K K_D bound to 25A

The reference number for the BMP2K K_D bound to 25A is PDB: 5IKW.